ARTICLE

https://doi.org/10.1038/s41586-018-0804-9

Structural basis of coreceptor recognition by HIV-1 envelope spike

Md Munan Shaik[1,2], Hanqin Peng[1], Jianming Lu[3,4], Sophia Rits-Volloch[1], Chen Xu[5], Maofu Liao[6] & Bing Chen[1,2]*

HIV-1 envelope glycoprotein (Env), which consists of trimeric $(gp160)_3$ cleaved to $(gp120 and gp41)_3$, interacts with the primary receptor CD4 and a coreceptor (such as chemokine receptor CCR5) to fuse viral and target-cell membranes. The gp120–coreceptor interaction has previously been proposed as the most crucial trigger for unleashing the fusogenic potential of gp41. Here we report a cryo-electron microscopy structure of a full-length gp120 in complex with soluble CD4 and unmodified human CCR5, at 3.9 Å resolution. The V3 loop of gp120 inserts into the chemokine-binding pocket formed by seven transmembrane helices of CCR5, and the N terminus of CCR5 contacts the CD4-induced bridging sheet of gp120. CCR5 induces no obvious allosteric changes in gp120 that can propagate to gp41; it does bring the Env trimer close to the target membrane. The N terminus of gp120, which is gripped by gp41 in the pre-fusion or CD4-bound Env, flips back in the CCR5-bound conformation and may irreversibly destabilize gp41 to initiate fusion. The coreceptor probably functions by stabilizing and anchoring the CD4-induced conformation of Env near the cell membrane. These results advance our understanding of HIV-1 entry into host cells and may guide the development of vaccines and therapeutic agents.

HIV-1 Env fuses viral and cell membranes, which enables the virus to enter host cells. gp160—the precursor of Env—trimerizes to form $(gp160)_3$, which is cleaved into two noncovalently associated fragments: gp120 (receptor-binding) and gp41 (fusion)[1]. Three copies of each fragment constitute the mature viral spike $(gp120 and gp41)_3$. Sequential binding of gp120 to the primary receptor CD4 and a coreceptor (for example, CCR5 or CXCR4) are believed to induce conformational changes that trigger the probable dissociation of gp120 and the refolding of gp41[1]. Structural rearrangements in gp41 bring the two membranes together, which promotes membrane fusion. Detailed structural information is available for the interaction of HIV-1 Env with CD4[2–6] but there is currently no molecular picture of the interaction between HIV-1 Env and a coreceptor, which continues to be the subject of speculative molecular modelling[7–10].

The chemokine receptors CCR5 and CXCR4 were identified as the HIV-1 coreceptors in 1996[11]. They are G-protein-coupled receptors with seven transmembrane-spanning segments. The choice of coreceptor is the major determinant for viral tropism[11]. Viruses that use CCR5 (R5 viruses) are generally responsible for viral transmission, and viruses that use CXCR4 (X4 viruses) or both coreceptors (dual-tropic; R5X4 viruses) emerge later during disease progression[12,13]. Both CCR5 and CXCR4 have an extracellular N-terminal segment, three extracellular loops (ECLs), three intracellular loops and a cytoplasmic C-terminal tail. Crystal structures have previously been reported for a C-terminally truncated CXCR4 (which also contains stabilizing mutations and a T4 lysozyme fusion) in complex with a range of different ligands, and for a similarly modified CCR5 that contains a rubredoxin fusion in complex with either an anti-HIV drug (maraviroc) or the modified chemokine [5P7]CCL5[7,10,14,15]. These structures show a typical helical bundle topology of seven transmembrane-spanning segments, seen in other G-protein-coupled receptors (Extended Data Fig. 1). Consistent with the so-called two-site model[16], the N-terminal segment of CXCR4 or CCR5 forms 'chemokine recognition site 1', which interacts with the globular core domain of chemokine; their bundle of seven transmembrane-spanning segments forms a binding pocket ('chemokine recognition site 2', CRS2) that accommodates the N terminus of the chemokine. Although these structures elucidate chemokine receptor function, they do not explain how CCR5 and CXCR4 function as HIV-1 coreceptors.

Mutagenesis studies have mapped the gp120-binding site to the N-terminal segment and ECL2 for CCR5, and to the N-terminal segment, ECL2 and ECL3 for CXCR4[17,18]. The footprint of the coreceptor on gp120 probably includes the V3 loop and the bridging sheet; this latter is a structure that is accessible only after CD4 binding[19,20]. The N terminus of the coreceptor may contact the bridging sheet of gp120, and the tip of the V3 loop may insert into the coreceptor CRS2[20]. Interactions of V3 with CCR5 or CXCR4 have also been modelled by molecular dynamics simulations and free energy calculations[7–10]. Tyrosine sulfation near the N terminus enhances HIV-1 entry for CCR5, but not for CXCR4[21,22]. The C-terminal tail, which contains palmitoylation and phosphorylation sites, is required for efficient cell signalling but not for HIV-1 coreceptor function[23]. Chemokines such as MIP-1α, MIP-1β, CCL5 (also known as RANTES) and CXCL12 (also known as SDF1) block gp120 binding and prevent viral infection[11].

Results

To understand how a coreceptor functions, we have determined the structure of an unmodified CCR5 in complex with a full-length HIV-1 gp120 and a four-domain soluble CD4 (hereafter, 'four-domain CD4') by single-particle cryo-electron microscopy (cryo-EM).

CCR5 complex purification and structure determination

To produce functional CCR5, we generated HEK293T or Expi293F cell lines that stably express wild-type human CCR5, using a previously published protocol[24]. The CCR5 in these cells was fully active as a chemokine receptor (Extended Data Fig. 2a), and formed a tight complex with HIV-1 gp120 in the presence of soluble CD4 (Extended Data Fig. 2b). Moreover, these cells fused efficiently with HIV-1 Env-expressing cells only when activated by soluble CD4 (Extended Data

[1]Division of Molecular Medicine, Boston Children's Hospital, Harvard Medical School, Boston, MA, USA. [2]Department of Pediatrics, Harvard Medical School, Boston, MA, USA. [3]Codex BioSolutions, Gaithersburg, MD, USA. [4]Xiamen Amoytop Biotech, Xiamen, China. [5]Cryo-EM Core Facility, University of Massachusetts Medical School, Worcester, MA, USA. [6]Department of Cell Biology, Harvard Medical School, Boston, MA, USA. *e-mail: bchen@crystal.harvard.edu

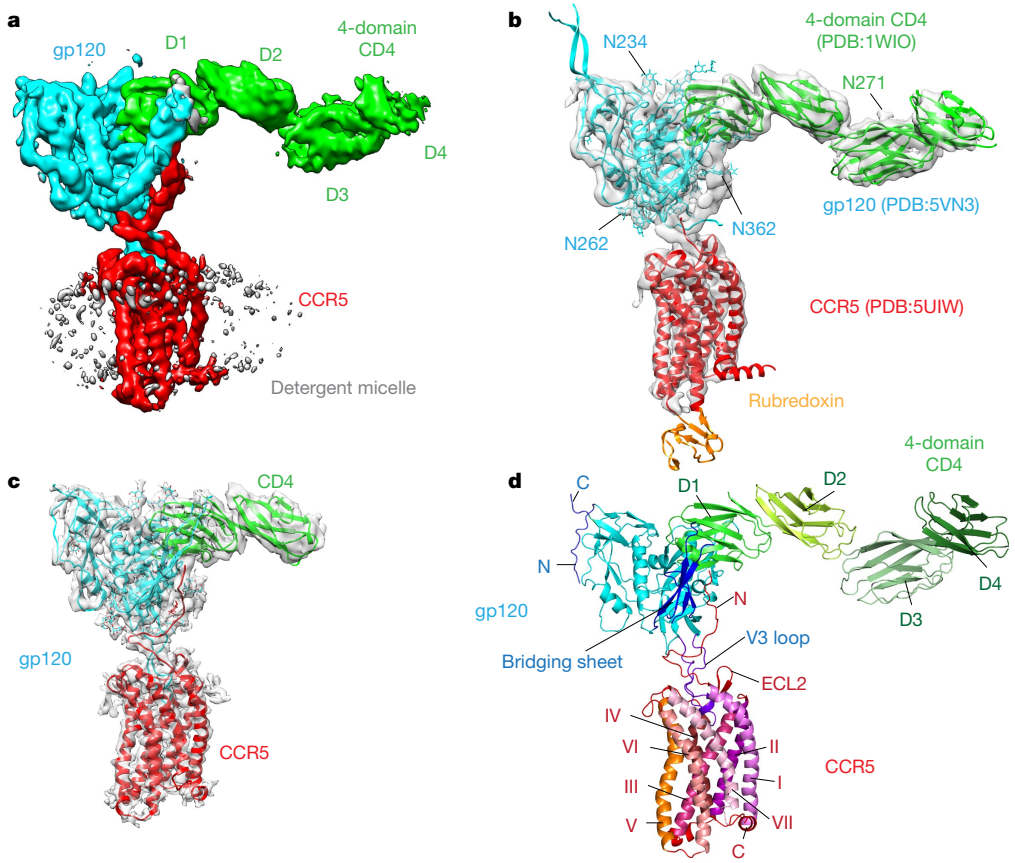

Fig. 1 | Cryo-EM structure of the CD4–gp120–CCR5 complex. **a**, Cryo-EM map of the complex that contains HIV-1 gp120 (cyan), CCR5 (red), four-domain CD4 (green; D1–D4, domain 1–domain 4) and detergent micelle (grey). **b**, Fit of structures of gp120 (RCSB Protein Data Bank code (PDB ID): 5VN3[28]), CCR5 (PDB ID: 5UIW[10]) and four-domain CD4 (PDB ID: 1WIO[27]) into the electron microscopy map shown in **a**. N271 of CD4 (green), N234, N262 and N362 of gp120 in cyan are *N*-linked glycosylation sites. **c**, The structure of the CD4–gp120–CCR5 complex was modelled on the basis of a 3.9 Å density map. **d**, Overall structure of the four-domain CD4–gp120–CCR5 complex shown in ribbon diagram. N, N terminus; C, C terminus; ECL2, extracellular loop 2; I, II, III, IV, V, VI, VII, transmembrane helices 1–7.

Fig. 2c), which suggests that the expressed CCR5 is a fully functional HIV-1 coreceptor. Finally, neither gp120 alone nor the gp120–CD4 complex could activate the G-protein mediated signalling pathways in these cells (Extended Data Fig. 2d, e).

To purify the wild-type CCR5 in its Env-bound conformation, we isolated the CD4–gp120–CCR5 complex from the CCR5-expressing cells (Extended Data Fig. 3a, b). The purified CD4–gp120–CCR5 complex eluted from a size-exclusion column as a single sharp peak at the expected volume, which confirmed its stability and conformational homogeneity (Extended Data Fig. 3c). Coomassie-stained sodium dodecyl sulfate–polyacrylamide gel electrophoresis and negative-stain electron microscopy of the peak fractions showed that all three components were in a stoichiometry of 1:1:1 (Extended Data Figs. 3c, 4a–c). The absence of any G proteins in the purified complex is consistent with the notion that gp120, unlike chemokines, does not require G-protein coupling for high-affinity binding to CCR5[25].

We acquired cryo-EM images on a Titan Krios electron microscope with a K2 Summit direct detector (Extended Data Fig. 4d) and used RELION[26] for image processing. Two-dimensional (2D) class averages of the particle images showed secondary structural features for both gp120 and CCR5 (Extended Data Fig. 4e). Three-dimensional (3D) classification of the particles was performed (Extended Data Fig. 5a), using the low-pass-filtered 3D reconstruction of the complex in negative stain as an initial model (Extended Data Fig. 4c). The particles from the classes with defined structural features were combined and refined to generate a map at 4.6 Å resolution, showing all three components (Extended Data Fig. 5a). The structure was determined by rounds of 3D classification, 3D classification with signal subtraction and masked refinement, as described in Methods and Extended Data Fig. 5a–d. The final resolution was 3.9 Å, when the last two domains of CD4 were excluded.

Overall structure of the CD4–gp120–CCR5 complex

The atomic structures of four-domain CD4[27], the gp120 core in complex with CD4[28], and the modified CCR5[10]—none of which was used in image processing—all fit as rigid bodies notably well to the electron microscopy density of the CD4–gp120–CCR5 at a 4.5 Å resolution (Fig. 1a, b and Extended Data Fig. 5b). The gp120 core, which contains inner and outer domains and the bridging sheet[2], occupied excellent density—this indicates that this region of gp120 has the same rigid structure in the ternary complex as it does in the CD4-induced conformation[2,28]. Several *N*-linked glycans were marked by protruding densities from the protein surfaces, as expected for a fully glycosylated gp120. All four domains of the soluble CD4 were visible, with density for first two (D1–D2) slightly stronger than for last two (D3–D4) domains. There was also density for an *N*-linked glycan at Asn271 in D3 (Fig. 1b), suggesting that the hinge region between D2 and D3 may not be very flexible[27]. All the helices of the seven transmembrane-spanning segments of CCR5 were well-resolved in detergent micelle. The palmitoylated cytoplasmic tail of CCR5, which presumably interacts with membrane, was disordered in this detergent-solubilized complex. Extra densities between CCR5 and gp120 that cannot be explained by the existing structures define the details of the interaction between CCR5 and gp120.

Interfaces between gp120 and CCR5

The map from the masked refinement showed good density for the gp120 and CCR5 interfaces (Fig. 1c and Extended Data Fig. 6). As previously postulated[7,14], there are two major contacting interfaces between gp120 and CCR5 (Fig. 1d). The V3 loop of gp120 inserts into the CRS2 of CCR5 and makes contact with all the helices of the seven transmembrane-spanning segments. The CCR5 N-terminal segment adopts an extended conformation with several sharp turns, and makes contact with the surface of the bridging sheet of gp120, which forms only after CD4 binding[2,28].

V3 loop of gp120 and CRS2 of CCR5

The conserved 310-Gly-Pro-Gly-Arg(Gln)-313 motif at the tip of the V3 loop penetrates by approximately one third of the thickness of the lipid bilayer into the CRS2 pocket; the Pro311 residue reaches most

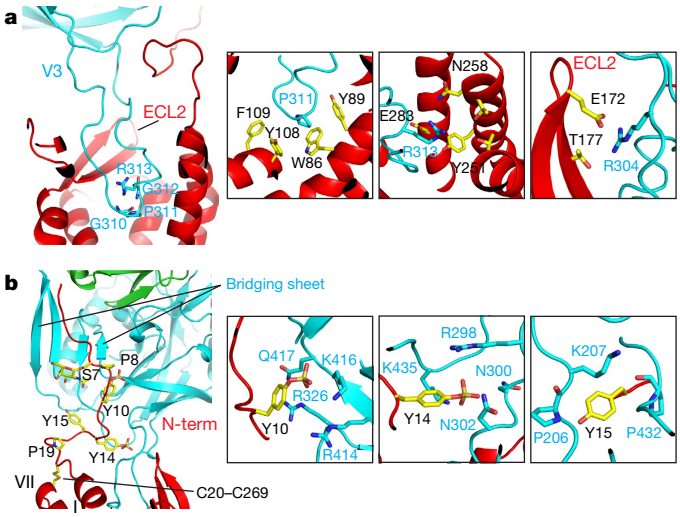

Fig. 2 | Interfaces between gp120 and CCR5. a, Interactions between the V3 loop of gp120 (cyan) and the CRS2 of CCR5 (red). Left, ribbon diagram of V3 inserting into the CRS2. The GPGR motif of V3 is in stick model. Right, major contacts between residues P311, R313 and R304 of gp120 (shown in cyan) and residues from CCR5. **b**, Interactions between the N terminus of CCR5 (red) and the bridging sheet of gp120 (cyan). Left, overall view of the N terminus of CCR5attaching to the four-stranded bridging sheet that is formed by the V1V2 stem and β21–β22 of gp120. Residues S7, P8, sulfated Y10 and Y14, Y15, P19, the *O*-linked glycan at S7, and the disulfide between C20 and C269 of CCR5 are shown in stick model. Right, major contacts between sulfated Y10 and Y14, as well as Y15, of CCR5 and residues from gp120.

deeply (Fig. 2a). Residues 309–316 of the V3 loop adopt a structure—including a one-turn helix—that is similar to that of the N terminus (residues 1–8) of [5P7]CCL5[10] (Extended Data Fig. 7a). Both of these structures have a proline residue (Pro311 of gp120 and Pro3 of [5P7]CCL5) that reaches the bottom of the CRS2, and which packs against the side chains of Trp86 and Tyr108 in CCR5 (Fig. 2a and Extended Data Fig. 7a). Arg313 in V3 appears to be sandwiched between Tyr251 and Glu283 of CCR5. The CRS2 of the chemokine receptors has minor and major subpockets formed by transmembrane helices I–III and VII and transmembrane helices III–VII, respectively[10]. The V3 loop of this HIV-1 strain occupies mainly the minor subpocket, and only a part of the major subpocket (Fig. 3a); this leaves room in the CRS2 to accommodate different V3 sequences from other viral isolates. Similar to [5P7]CCL5, different V3 loops may also have water-mediated interactions with CCR5[10]. The ECL2 of CCR5 forms a nearly semi-circular grip as it wraps around V3, and makes contacts with residues in both the V3 stem and crown[29]. In particular, Glu172 in ECL2 and Arg304 in V3 probably form a salt bridge (Fig. 2a). Overall, the gp120 V3 loop makes extensive contacts with the CRS2 of CCR5, which contributes to the high affinity of HIV-1 Env for its coreceptor.

The gp120 bridging sheet and CCR5 N terminus

The second major interface between Env and its coreceptor is formed by the N terminus of CCR5 and the bridging sheet of gp120. Helices I and VII of CCR5 are locked by a disulfide (Cys20–Cys269); the N-terminal segment (residues 1–19), which is connected to helix I, is largely disordered in the crystal structures of CCR5 in complex with other ligands[7,10]. In the CD4–gp120–CCR5 complex, the N-terminal segment adopts an extended conformation with several sharp turns and attaches to the surface of the bridging sheet, which is formed by the V1V2 stem and the β20–β21 hairpin, upon CD4 binding (Fig. 2b). Three tyrosine residues (Tyr10, Tyr14 and Tyr15) of CCR5—all of which can be sulfated[21]—make the most intimate contacts with gp120. There appears to be density and room for sulfate groups on Tyr10 and Tyr14, but not on Tyr15 (Extended Data Fig. 6). The aromatic ring of sulfated Tyr10 packs against the side chain of Arg326 in gp120—probably via a cation-π interaction[30]; this places the putative sulfate group near the Lys416 and Arg414 of gp120. Sulfated Tyr14 wedges between the bases of both the V3 stem and the bridging sheet, positioning its sulfate group near the side chains of the Arg 298 and Lys 435 of gp120. The side chain of Tyr15 is close to Lys207 at the base of the V1V2 stem, where they potentially form another cation-π interaction. Sulfated Tyr10 and Tyr14 mimic the interactions with gp120 of two sulfated tyrosines, Tyr100 and Tyr100c, in antibody 412d[20] (Extended Data Fig. 7b). There also appears to be an *O*-linked glycan at Ser7, a previously identified glycosylation site[31], and the carbohydrate may help to maintain the configuration of the N-terminal region of CCR5.

One unexpected feature of the complex structure is the orientation of CD4 relative to the helices of the seven transmembrane-spanning segments of CCR5. The long axis of CD4 lies almost perpendicular to the axis of the CCR5 transmembrane helices and roughly parallel to the plane of the lipid bilayer, which raises the possibility that the formation of the ternary complex could induce a local bend in the membrane. Although the binding of an Env trimer to three copies each of CD4 and CCR5 simultaneously is stereochemically possible (Extended Data Fig. 7c), it may be an inefficient process if such a stoichiometry is needed to activate gp41.

Conformation of CCR5 bound by different ligands

There is no published structure for CCR5 in the absence of ligand, as the structure may be conformationally flexible, and sample a range of conformations even in its native membrane environment[32]. In a complex with CCR5 stabilized by specific mutations, maraviroc binds in a hydrophobic pocket near the bottom of CRS2; the drug has previously been thought to inhibit HIV-1 infection by stabilizing a conformation that Env cannot recognize[33]. However, we find that the overall dimension and shape of the gp120-bound CRS2 pocket from the wild-type CCR5 are not very different from those of other liganded CCR5s with stabilizing modifications (Fig. 3a). A comparison of the structures of the CCR5–maraviroc and CCR5–gp120 complexes indicates that the parts of all transmembrane helices near the intracellular side—including transmembrane helix 6, which is critical for the activation of G-protein-coupled receptors[34]—show few differences, which indicates that the gp120-bound CCR5 also adopts an inactive conformation (Extended Data Fig. 7d). Indeed, the binding of the gp120–CD4 complex did not activate the G-protein-signalling pathways (Extended Data Fig. 2d, e). The parts of CCR5 that are near the extracellular surface move outwards by between 1 and 3 Å to accommodate the inserted V3 loop (Fig. 3b). The largest changes are in the long β-hairpin of ECL2: part of the body of this hairpin moves outwards by beween 2 and 3 Å, and its tip moves inwards by more than 5 Å to tight its grip on the V3 loop. However, these conformational differences are unlikely to block the access of the V3 loop to the CRS2 pocket. In addition, the binding site of maraviroc partially overlaps with that of the V3 tip, which suggests that the drug blocks gp120 binding by direct competition rather than by restricting conformational availability. Moreover, the CCR5 with stabilizing mutations bound to the antagonist [5P7]CCL5 also adopts a conformation very similar to that of the gp120-bound wild-type CCR5, which suggests that the conformational freedom of the transmembrane helices of CCR5 is limited, at least in the liganded inactive forms (Fig. 3c).

Differences between CD4- and CCR5-bound gp120

The most unexpected aspect of the CD4–gp120–CCR5 structure is the absence of obvious allosteric changes that can propagate from the CCR5-binding site to gp41, as previously hypothesized. Whereas CD4 and/or CD4i antibody-induced conformational changes in the SOSIP-based Env trimer have recently been described[28], a comparison of the CD4- and CCR5-bound gp120 with the CD4-bound gp120 shows no major differences in the core region of gp120 (Fig. 4a and Extended Data Fig. 8a). In particular, an approximately 50 Å zone between the CCR5-binding site and the gp120–gp41 interface (including the inner

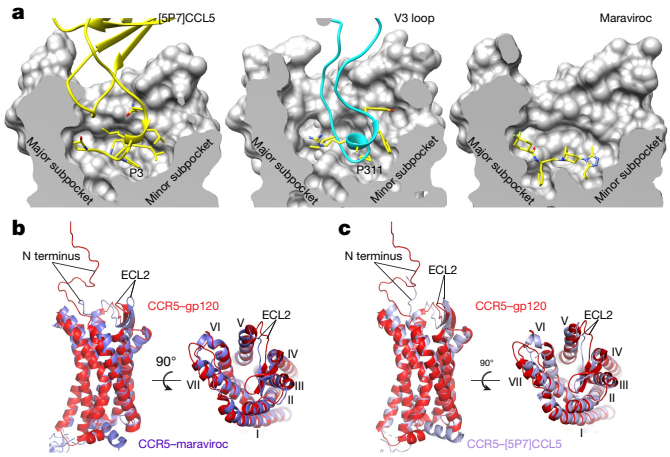

Fig. 3 | Conformational differences between gp120-bound CCR5 and CCR5 bound to other ligands. a, The section of the CRS2 of CCR5 (divided into a major and a minor subpocket) is shown in surface representation for the [5P7]CCL5, gp120 and maraviroc complexes. Interacting residues—including P3 from [5P7]CCL5, P311 from the V3 loop and the compound maraviroc—are shown in stick model. **b**, Superposition of the structures of the gp120–CCR5 complex (red) and the maraviroc–CCR5 complex (blue). The N terminus, ELC2 and seven transmembrane helices (I, II, III, IV, V, VI, VII) are indicated. **c**, Superposition of the structures of the gp120–CCR5 complex (red) and the [5P7]CCL5–CCR5 complex (blue).

and outer domains and the bridging sheet) remains almost invariant, which suggests that CCR5 does not induce any major structural changes that affect gp41. There are, however, some differences between the two structures. First, when CCR5 binds the V3 loop reconfigures to fit into the CRS2 pocket (Fig. 3a). This conformation, which partially mimics that of the N terminus of [5P7]CCL5, has not been seen for either unliganded or antibody-bound V3 loops[20,35–38] (Extended Data Fig. 8b). Second, a more substantial difference is seen in the region that includes the N and C termini of gp120, near its interface with gp41. In the pre-fusion SOSIP trimer structure, the gp120 termini are surrounded by the so-called 'four-helix collar' of gp41, which closes by insertion of the side chain of Met530—located on one of the helices (α6)—into a hydrophobic clasp formed by three tryptophan residues on two other helices (α8 and α9)[5]. CD4 binding induces a shift of α6, which enables the fusion peptide to pack directly against the termini of gp120[28] (Fig. 4b). In the CD4–gp120–CCR5 complex, the N and C termini bend back at pivot regions that contain the highly conserved 40-Gly-Val-Pro-42 and 489-Pro-Leu-Gly-491 sequences, respectively. In particular, the N terminus rotates almost by about 180° to pack against the surface of gp120 and occupies the space of the fusion peptide in the Env trimer (Fig. 4b). There is no obvious density for the rest of the C terminus, which is probably disordered—although the histidine tag could influence its conformation.

Model for how CCR5 functions as an HIV-1 coreceptor

Because CCR5 binding does not appear to induce any allosteric changes that can unleash gp41 to fuse membranes, it is intriguing how CCR5 might function as an essential coreceptor. On the basis of the known structures of the HIV-1 Env trimer[3–5,28,39], the pre-fusion gp41—which wraps around the N and C termini of gp120—is no longer stable and is likely to enter an irreversible refolding process once gp120 dissociates. Thus, gp120 dissociation may be the crucial trigger that initiates gp41 refolding events, including the insertion of the fusion peptide of gp41 into the target membrane and the formation of the post-fusion conformation. In the pre-fusion conformation, the N and C termini of gp120 are gripped by the four-helix collar of gp41[5]. CD4 binding leads to a large shift of the C terminus of helix α6 away from the gp120 termini; this creates a pocket, which is filled by the fusion peptide[28] that packs against the pivot region (^{40}Gly-Val-Pro^{42}) of the gp120 N terminus (Fig. 4b). When intrinsic conformational dynamics cause the fusion peptide to dissociate from the pocket, this opens up one side of the gp41 grip, and the gp120 N terminus can then bend back to adopt the conformation observed in the CCR5-bound structure (Extended Data Fig. 9). The rearrangements of the termini of gp120—which are probably independent of CCR5 binding—can prevent the fusion peptide from reoccupying the pocket and effectively weaken gp120–gp41 interactions, which possibly leads to complete dissociation. Indeed, spontaneous or CD4-induced gp120 shedding from Env trimers are well-documented for many HIV-1 isolates[40,41], which indicates that gp120 is prone to dissociation from gp41 even in the absence of a coreceptor. We note that the effect of the membranes and Env trimer organization remains unknown and will require further investigation.

If the rearrangement of gp120 termini to activate gp41 does not depend on CCR5 binding, the question arises as to why a coreceptor would be needed at all. First, premature gp120 dissociation would—in absence of a coreceptor—be non-productive; for a virion attached to the target-cell surface only through an Env trimer–CD4 contact, the distance between the fusion peptide and membrane surface can be about 160 Å (Fig. 4b). If gp120 dissociates, the fusion peptide would be too far away to reach the target membrane. The binding of gp120 to CCR5 can bring the fusion peptide of gp41 to within 70 Å of the membrane surface (Fig. 4b), which is consistent with the distance needed for the fusion peptide to translocate and reach the target membrane[5]. Second, the gp120–CD4 association—measured by single-molecule force spectroscopy with infectious virions and live host cells—is unstable, and rapidly reversible unless CCR5 binding follows immediately[42,43]. CCR5 is therefore needed to stabilize the CD4-induced conformational changes, which are already competent for promoting fusion. In particular, the tucking away of the V3 loop by CCR5 would prevent the Env trimer from moving back to the pre-fusion conformation, and help shift the equilibrium towards the irreversible step—that is, gp41 refolding. Third, membrane fusion may require more than one Env trimer to induce fusion pore formation[44], as shown for other viral fusion proteins[45]. Because the number of Env trimers on the virion is low—about 14 trimers per virion[46]—a long lifetime for the Env–receptor complex would be important for recruiting additional CD4- and coreceptor-primed trimers. Thus, our structure shows how a coreceptor can be essential for membrane fusion, despite the fact that it does not actively induce gp41 refolding.

Coreceptor switch

The switch from CCR5 to CXCR4 is often associated with an accelerated increase in viral load and decrease in $CD4^+$ T cells, as well as with faster disease progression[12,13]. Our structure supports a model for how simple mutations in Env can achieve this seemingly complicated transition. First, the coreceptor is required only to stabilize the CD4-induced conformation, and not to trigger additional allosteric changes in Env through specific interactions. The switch can thus be accomplished if the V3 loop gains sufficient affinity for CXCR4 and does not release the coreceptor, as no specific mutations in Env are needed to make it able to be 'triggered' by CXCR4. Second, the overall dimensions of the CRS2 pocket in the gp120-bound CCR5 and the liganded CXCR4 are very similar[14,15] (Extended Data Fig. 1), which suggests that changes of the surface-exposed residues in the V3 loop to make it compatible with CXCR4 binding would be sufficient. Use of both coreceptors by R5X4 isolates further underscores the similarities between the two coreceptors[11]. Third, the main contacts between gp120 and the CCR5 N terminus are electrostatic. CXCR4 has seven acidic residues in its N terminus (before the first disulfide-forming Cys residue) and CCR5 has four, in addition to two or three sulfotyrosines. No additional mutations in the bridging sheet region would be needed if the extra acidic residues in CXCR4 can replace the two critical sulfated tyrosines in CCR5. Finally, X4 V3 loops generally have more positive charges than those of R5 viruses, consistent with a more negatively charged CRS2 in CXCR4 than CCR5. Evolution from CCR5 to CXCR4 use can indeed be achieved by multiple mutational pathways, but often gain net positive charges in the V3 region[47–49].

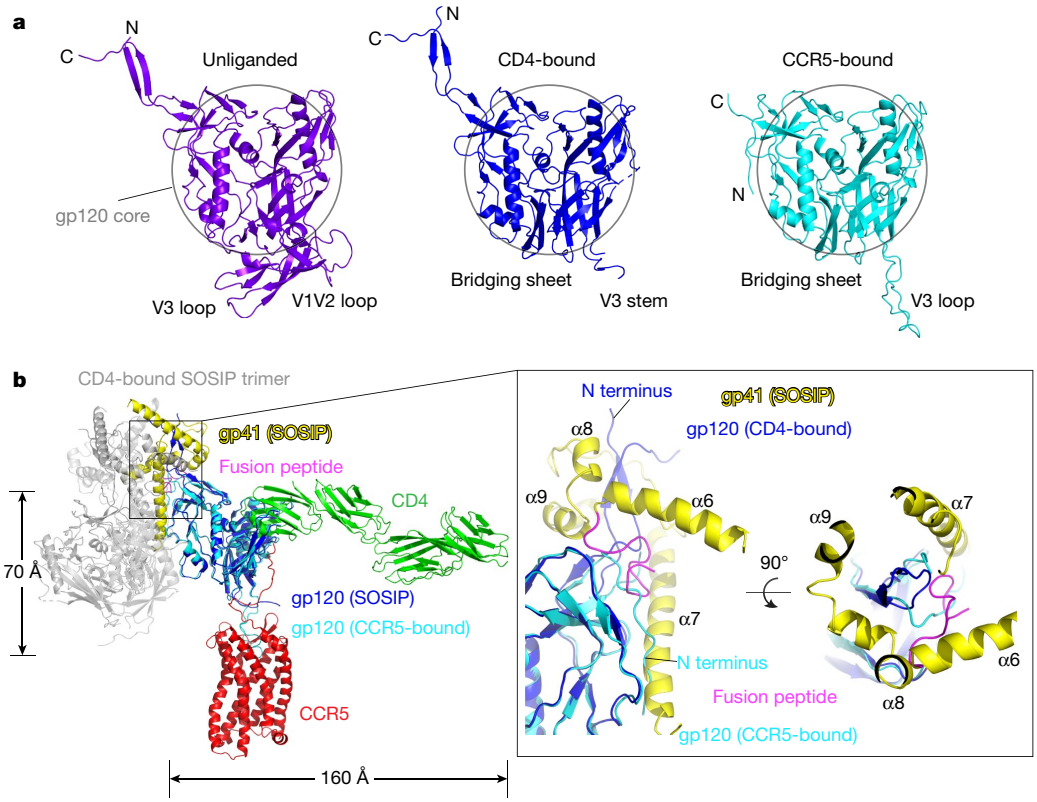

Fig. 4 | Conformational differences between CD4-bound and CCR5-bound gp120. a, Comparison of structures of gp120 in the unliganded SOSIP Env trimer (PDB ID: 4ZMJ[35]; purple), in the CD4-bound SOSIP trimer (PDB ID:5VN3[28]; blue) and in complex with CD4 and CCR5 (cyan). A 50 Å circle marks the core region of gp120. **b**, Superposition of structures of the CD4–gp120–CCR5 complex and the CD4-bound SOSIP trimer. Left, the two structures are superposed by the core region of gp120 and the first two domains of CD4. CCR5-bound gp120 is in cyan, CCR5 is in red and CD4 is in green; one of the gp120 subunits from the trimer is shown in blue and the corresponding gp41 is in yellow (except for its fusion peptide, which is shown in magenta). The rest of the SOSIP trimer is shown in grey. The distances between the fusion peptide and the transmembrane domains of CD4 and CCR5 are 160 Å and 70 Å, respectively. Right, close-up views of the gp120 N- and C-terminal regions. The four helices (α6, α7, α8 and α9) of gp41 that form the four-helix collar are indicated. The N terminus of the CCR5-bound gp120 overlaps with the fusion peptide in the CD4-bound trimer.

Therapeutic agents based on CCR5 antagonists

The V3 binding-site only partially overlaps with the minor subpocket of the maraviroc binding-site (Fig. 3a). Maraviroc-resistant viruses can emerge either in infected individuals under the treatment, or by in vitro selection. Major changes in the escaped viruses map to the V3 region—some of these changes have a three-residue deletion, but in general they show no consistent patterns[50–52]. Some resistant viruses can infect cells by recognizing the drug-bound CCR5[50,53]. In addition, replication-competent HIV-2 viruses have been selected that lack the entire V3 loop[54]. These viruses can use both coreceptors for entry, by gaining additional positively charged residues near the bridging sheet to enhance interactions with the coreceptor N terminus. These data indicate that no specific structural determinants in the V3 region are required for the coreceptor to function, which is fully consistent with our conclusion that CCR5 does not actively trigger gp41 through specific interactions with gp120.

Our structure also suggests a general strategy for how to improve maraviroc-like therapeutic agents. Because the V3 loop mainly overlaps with maraviroc in the minor subpocket (which is primarily occupied by the triazole group of the compound), additional groups may be added to the triazole ring to enhance its competing power with the V3 loop and increase the barrier to drug resistance.

Online content

Any methods, additional references, Nature Research reporting summaries, source data, statements of data availability and associated accession codes are available at https://doi.org/10.1038/s41586-018-0804-9.

Received: 5 July 2018; Accepted: 2 November 2018;
Published online 12 December 2018.

1. Harrison, S. C. Viral membrane fusion. *Nat. Struct. Mol. Biol.* **15**, 690–698 (2008).
2. Kwong, P. D. et al. Structure of an HIV gp120 envelope glycoprotein in complex with the CD4 receptor and a neutralizing human antibody. *Nature* **393**, 648–659 (1998).
3. Julien, J. P. et al. Crystal structure of a soluble cleaved HIV-1 envelope trimer. *Science* **342**, 1477–1483 (2013).
4. Lee, J. H., Ozorowski, G. & Ward, A. B. Cryo-EM structure of a native, fully glycosylated, cleaved HIV-1 envelope trimer. *Science* **351**, 1043–1048 (2016).
5. Pancera, M. et al. Structure and immune recognition of trimeric pre-fusion HIV-1 Env. *Nature* **514**, 455–461 (2014).
6. Wang, H. et al. Cryo-EM structure of a CD4-bound open HIV-1 envelope trimer reveals structural rearrangements of the gp120 V1V2 loop. *Proc. Natl Acad. Sci. USA* **113**, E7151–E7158 (2016).
7. Tan, Q. et al. Structure of the CCR5 chemokine receptor-HIV entry inhibitor maraviroc complex. *Science* **341**, 1387–1390 (2013
8. Tamamis, P. & Floudas, C. A. Molecular recognition of CXCR4 by a dual tropic HIV-1 gp120 V3 loop. *Biophys. J.* **105**, 1502–1514 (2013).
9. Tamamis, P. & Floudas, C. A. Molecular recognition of CCR5 by an HIV-1 gp120 V3 loop. *PLoS ONE* **9**, e95767 (2014).
10. Zheng, Y. et al. Structure of CC chemokine receptor 5 with a potent chemokine antagonist reveals mechanisms of chemokine recognition and molecular mimicry by HIV. *Immunity* **46**, 1005–1017.e1005 (2017).
11. Berger, E. A., Murphy, P. M. & Farber, J. M. Chemokine receptors as HIV-1 coreceptors: roles in viral entry, tropism, and disease. *Annu. Rev. Immunol.* **17**, 657–700 (1999).
12. Connor, R. I., Sheridan, K. E., Ceradini, D., Choe, S. & Landau, N. R. Change in coreceptor use correlates with disease progression in HIV-1–infected individuals. *J. Exp. Med.* **185**, 621–628 (1997).
13. Verhofstede, C., Nijhuis, M. & Vandekerckhove, L. Correlation of coreceptor usage and disease progression. *Curr. Opin. HIV AIDS* **7**, 432–439 (2012).
14. Wu, B. et al. Structures of the CXCR4 chemokine GPCR with small-molecule and cyclic peptide antagonists. *Science* **330**, 1066–1071 (2010).
15. Qin, L. et al. Crystal structure of the chemokine receptor CXCR4 in complex with a viral chemokine. *Science* **347**, 1117–1122 (2015).
16. Scholten, D. J. et al. Pharmacological modulation of chemokine receptor function. *Br. J. Pharmacol.* **165**, 1617–1643 (2012).

17. Lin, G., Baribaud, F., Romano, J., Doms, R. W. & Hoxie, J. A. Identification of gp120 binding sites on CXCR4 by using CD4-independent human immunodeficiency virus type 2 Env proteins. *J. Virol.* **77**, 931–942 (2003).
18. Doranz, B. J. et al. Two distinct CCR5 domains can mediate coreceptor usage by human immunodeficiency virus type 1. *J. Virol.* **71**, 6305–6314 (1997).
19. Rizzuto, C. D. et al. A conserved HIV gp120 glycoprotein structure involved in chemokine receptor binding. *Science* **280**, 1949–1953 (1998).
20. Huang, C. C. et al. Structures of the CCR5 N terminus and of a tyrosine-sulfated antibody with HIV-1 gp120 and CD4. *Science* **317**, 1930–1934 (2007).
21. Farzan, M. et al. Tyrosine sulfation of the amino terminus of CCR5 facilitates HIV-1 entry. *Cell* **96**, 667–676 (1999).
22. Farzan, M. et al. The role of post-translational modifications of the CXCR4 amino terminus in stromal-derived factor 1α association and HIV-1 entry. *J. Biol. Chem.* **277**, 29484–29489 (2002).
23. Oppermann, M. Chemokine receptor CCR5: insights into structure, function, and regulation. *Cell. Signal.* **16**, 1201–1210 (2004).
24. Chen, J. et al. Effect of the cytoplasmic domain on antigenic characteristics of HIV-1 envelope glycoprotein. *Science* **349**, 191–195 (2015).
25. Colin, P. et al. HIV-1 exploits CCR5 conformational heterogeneity to escape inhibition by chemokines. *Proc. Natl Acad. Sci. USA* **110**, 9475–9480 (2013).
26. Scheres, S. H. RELION: implementation of a Bayesian approach to cryo-EM structure determination. *J. Struct. Biol.* **180**, 519–530 (2012).
27. Wu, H., Kwong, P. D. & Hendrickson, W. A. Dimeric association and segmental variability in the structure of human CD4. *Nature* **387**, 527–530 (1997).
28. Ozorowski, G. et al. Open and closed structures reveal allostery and pliability in the HIV-1 envelope spike. *Nature* **547**, 360–363 (2017).
29. Huang, C. C. et al. Structure of a V3-containing HIV-1 gp120 core. *Science* **310**, 1025–1028 (2005).
30. Gallivan, J. P. & Dougherty, D. A. Cation-π interactions in structural biology. *Proc. Natl Acad. Sci. USA* **96**, 9459–9464 (1999).
31. Bannert, N. et al. Sialylated O-glycans and sulfated tyrosines in the NH2-terminal domain of CC chemokine receptor 5 contribute to high affinity binding of chemokines. *J. Exp. Med.* **194**, 1661–1673 (2001).
32. Berro, R. et al. Multiple CCR5 conformations on the cell surface are used differentially by human immunodeficiency viruses resistant or sensitive to CCR5 inhibitors. *J. Virol.* **85**, 8227–8240 (2011).
33. Moore, J. P. & Kuritzkes, D. R. A pièce de resistance: how HIV-1 escapes small molecule CCR5 inhibitors. *Curr. Opin. HIV AIDS* **4**, 118–124 (2009).
34. Manglik, A. & Kruse, A. C. Structural basis for G protein-coupled receptor activation. *Biochemistry* **56**, 5628–5634 (2017).
35. Kwon, Y. D. et al. Crystal structure, conformational fixation and entry-related interactions of mature ligand-free HIV-1 Env. *Nat. Struct. Mol. Biol.* **22**, 522–531 (2015).
36. Burke, V. et al. Structural basis of the cross-reactivity of genetically related human anti-HIV-1 mAbs: implications for design of V3-based immunogens. *Structure* **17**, 1538–1546 (2009).
37. Jiang, X. et al. Conserved structural elements in the V3 crown of HIV-1 gp120. *Nat. Struct. Mol. Biol.* **17**, 955–961 (2010).
38. Pan, R. et al. Increased epitope complexity correlated with antibody affinity maturation and a novel binding mode revealed by structures of rabbit antibodies against the third variable loop (V3) of HIV-1 gp120. *J. Virol.* e01894-17 (2018).
39. Lyumkis, D. et al. Cryo-EM structure of a fully glycosylated soluble cleaved HIV-1 envelope trimer. *Science* **342**, 1484–1490 (2013).
40. Moore, J. P., McKeating, J. A., Weiss, R. A. & Sattentau, Q. J. Dissociation of gp120 from HIV-1 virions induced by soluble CD4. *Science* **250**, 1139–1142 (1990).
41. Thali, M., Furman, C., Helseth, E., Repke, H. & Sodroski, J. Lack of correlation between soluble CD4-induced shedding of the human immunodeficiency virus type 1 exterior envelope glycoprotein and subsequent membrane fusion events. *J. Virol.* **66**, 5516–5524 (1992).
42. Chang, M. I., Panorchan, P., Dobrowsky, T. M., Tseng, Y. & Wirtz, D. Single-molecule analysis of human immunodeficiency virus type 1 gp120-receptor interactions in living cells. *J. Virol.* **79**, 14748–14755 (2005).
43. Dobrowsky, T. M., Zhou, Y., Sun, S. X., Siliciano, R. F. & Wirtz, D. Monitoring early fusion dynamics of human immunodeficiency virus type 1 at single-molecule resolution. *J. Virol.* **82**, 7022–7033 (2008).
44. Brandenberg, O. F., Magnus, C., Regoes, R. R. & Trkola, A. The HIV-1 entry process: a stoichiometric view. *Trends Microbiol.* **23**, 763–774 (2015).
45. Floyd, D. L., Ragains, J. R., Skehel, J. J., Harrison, S. C. & van Oijen, A. M. Single-particle kinetics of influenza virus membrane fusion. *Proc. Natl Acad. Sci. USA* **105**, 15382–15387 (2008).
46. Zhu, P. et al. Distribution and three-dimensional structure of AIDS virus envelope spikes. *Nature* **441**, 847–852 (2006).
47. Rosen, O., Sharon, M., Quadt-Akabayov, S. R. & Anglister, J. Molecular switch for alternative conformations of the HIV-1 V3 region: implications for phenotype conversion. *Proc. Natl Acad. Sci. USA* **103**, 13950–13955 (2006).
48. Ho, S. H., Trunova, N., Gettie, A., Blanchard, J. & Cheng-Mayer, C. Different mutational pathways to CXCR4 coreceptor switch of CCR5-using simian-human immunodeficiency virus. *J. Virol.* **82**, 5653–5656 (2008).
49. Edo-Matas, D., van Dort, K. A., Setiawan, L. C., Schuitemaker, H. & Kootstra, N. A. Comparison of *in vivo* and *in vitro* evolution of CCR5 to CXCR4 coreceptor use of primary human immunodeficiency virus type 1 variants. *Virology* **412**, 269–277 (2011).
50. Westby, M. et al. Reduced maximal inhibition in phenotypic susceptibility assays indicates that viral strains resistant to the CCR5 antagonist maraviroc utilize inhibitor-bound receptor for entry. *J. Virol.* **81**, 2359–2371 (2007).
51. Seclén, E. et al. Primary resistance to maraviroc in a large set of R5-V3 viral sequences from HIV-1-infected patients. *J. Antimicrob. Chemother.* **65**, 2502–2504 (2010).
52. Jiang, X. et al. Characterizing the diverse mutational pathways associated with R5-tropic maraviroc resistance: HIV-1 that uses the drug-bound CCR5 coreceptor. *J. Virol.* **89**, 11457–11472 (2015).
53. Pugach, P. et al. HIV-1 clones resistant to a small molecule CCR5 inhibitor use the inhibitor-bound form of CCR5 for entry. *Virology* **361**, 212–228 (2007).
54. Lin, G. et al. Replication-competent variants of human immunodeficiency virus type 2 lacking the V3 loop exhibit resistance to chemokine receptor antagonists. *J. Virol.* **81**, 9956–9966 (2007).
55. Zolla-Pazner, S. et al. The cross-clade neutralizing activity of a human monoclonal antibody is determined by the GPGR V3 motif of HIV type 1. *AIDS Res. Hum. Retroviruses* **20**, 1254–1258 (2004).
56. Frey, G. et al. A fusion-intermediate state of HIV-1 gp41 targeted by broadly neutralizing antibodies. *Proc. Natl Acad. Sci. USA* **105**, 3739–3744 (2008).
57. Kovacs, J. M. et al. HIV-1 envelope trimer elicits more potent neutralizing antibody responses than monomeric gp120. *Proc. Natl Acad. Sci. USA* **109**, 12111–12116 (2012).
58. Freeman, M. M. et al. Crystal structure of HIV-1 primary receptor CD4 in complex with a potent antiviral antibody. *Structure* **18**, 1632–1641 (2010).
59. Cai, Y. et al. Antigenicity-defined conformations of an extremely neutralization-resistant HIV-1 envelope spike. *Proc. Natl Acad. Sci. USA* **114**, 4477–4482 (2017).
60. Brady, A. E. & Limbird, L. E. G protein-coupled receptor interacting proteins: emerging roles in localization and signal transduction. *Cell. Signal.* **14**, 297–309 (2002).
61. Visegrády, A., Boros, A., Némethy, Z., Kiss, B. & Keseru, G. M. Application of the BD ACT*One*™ technology for the high-throughput screening of G_s-coupled receptor antagonists. *J. Biomol. Screen.* **12**, 1068–1073 (2007).
62. Melar, M., Ott, D. E. & Hope, T. J. Physiological levels of virion-associated human immunodeficiency virus type 1 envelope induce coreceptor-dependent calcium flux. *J. Virol.* **81**, 1773–1785 (2007).
63. Tang, G. et al. EMAN2: an extensible image processing suite for electron microscopy. *J. Struct. Biol.* **157**, 38–46 (2007).
64. Ru, H. et al. Molecular mechanism of V(D)J recombination from synaptic RAG1–RAG2 complex structures. *Cell* **163**, 1138–1152 (2015).
65. Mastronarde, D. N. Automated electron microscope tomography using robust prediction of specimen movements. *J. Struct. Biol.* **152**, 36–51 (2005).
66. Zheng, S. Q. et al. MotionCor2: anisotropic correction of beam-induced motion for improved cryo-electron microscopy. *Nat. Methods* **14**, 331–332 (2017).
67. Rohou, A. & Grigorieff, N. CTFFIND4: Fast and accurate defocus estimation from electron micrographs. *J. Struct. Biol.* **192**, 216–221 (2015).
68. Roy, A., Kucukural, A. & Zhang, Y. I-TASSER: a unified platform for automated protein structure and function prediction. *Nat. Protocols* **5**, 725–738 (2010).
69. Emsley, P., Lohkamp, B., Scott, W. G. & Cowtan, K. Features and development of Coot. *Acta Crystallogr. D* **66**, 486–501 (2010).
70. Adams, P. D. et al. PHENIX: a comprehensive Python-based system for macromolecular structure solution. *Acta Crystallogr. D* **66**, 213–221 (2010).

Acknowledgements We thank S. Harrison and A. Kruse for advice, K. Song, J. Chen, R. Martin and W. Chang for technical assistance, N. Grigorieff and T. Grant for discussion at the early stage of the project, and S. Harrison and A. Kruse for critical reading of the manuscript. This work was supported by NIH grants AI141002 (to B.C.), AI106488 (to B.C.), AI129721 (to B.C.), AI127193 (to B.C. and J.J.C.), the Center for HIV/AIDS Vaccine Immunology - Immunogen Design AI-100645 (to B. F. Haynes), and Collaboration for AIDS Vaccine Discovery (CAVD) grant OPP1169339 (to D. H. Barouch from the Bill and Melinda Gates Foundation).

Reviewer information *Nature* thanks G. Melikyan, S. Subramaniam and the other anonymous reviewer(s) for their contribution to the peer review of this work.

Author contributions B.C. and M.M.S. designed the experiments. H.P. and M.M.S. purified the CD4–gp120–CCR5 complex. J.L. performed CCR5 chemokine receptor assays. M.M.S. and S.R.-V. carried out CCR5 coreceptor functional assays. M.M.S. performed electron microscopy data collection with contributions from C.X. M.L. processed the initial negative-stain data. M.M.S. processed the cryo-EM data with contributions from M.L., and built the atomic model with help from B.C. All authors analysed the data. B.C. and M.M.S. wrote the manuscript with input from M.L. and J.L.

Competing interests The authors declare no competing interests.

Additional information

Extended data is available for this paper at https://doi.org/10.1038/s41586-018-0804-9.
Supplementary information is available for this paper at https://doi.org/10.1038/s41586-018-0804-9.

Correspondence and requests for materials should be addressed to B.C.

METHODS

No statistical methods were used to predetermine sample size. The experiments were not randomized and investigators were not blinded to allocation during experiments and outcome assessment.

Constructs and stable cell lines. The gene of the intact human C-C chemokine receptor type 5 (CCR5; NCBI reference sequence: NP_000570.1) was cloned into pCMV-IRES-puro vector (Codex BioSolutions). Genes of HIV-1 gp120 (residues 1–507) from the isolate 92BR020 with a C-terminal 6×histidine tag, and of four-domain CD4 (residues 1–388) with a C-terminal twin strep tag [$(GGGGS)_2$WSHPQFEK$(GGGGS)_2$WSHPQFEK)] were synthesized by GenScript and cloned into pCMV-IRES-puro vector. HEK293T cell lines (Thermo Fisher Scientific) that were stably transfected (HEK293T-CCR5) with these constructs were generated either in-house or at Codex Biosolutions. In brief, 8×10^5 HEK293T cells in 2 ml of DMEM containing 10% FBS and no antibiotics were seeded on a 6-well plate and incubated overnight. The cells were then transfected with the expression constructs using DNA-In 293 Transfection Reagent (MTI-GlobalStem), following a protocol recommended by the manufacturer. Twenty-four hours after transfection, the cells were transferred to a medium containing DMEM, 10% FBS and 1 μg/ml puromycin for selection. Single colonies were picked after 2–3 weeks, and transferred to 24-well plates in the same selective medium. Protein expression was confirmed by both western blot and a fluorescence-activated cell sorting assay (see below). Positive clones were expanded, frozen and stored in liquid nitrogen. To grow cells in large-scale in suspension, we also generated stable cell lines expressing CCR5 with Expi293F (Expi293F-CCR5) cells (Thermo Fisher Scientific). Hybridoma cells for production of an anti-V3 antibody 447-52D[55] were provided by S. Zolla-Pazner (New York University). Each cell line was authenticated for protein expression by western blot and/or flow cytometry, and other functional assays, such as cell-cell fusion and chemokine receptor assays. Our cell culture is routinely tested for mycoplasma contamination.

Purification of recombinant proteins. *HIV-1 gp120 of the isolate 92BR020.* Cells that express C-terminal His-tagged 92BR020 gp120 were grown in 250-ml roller bottles with DMEM containing 10% FBS and 1 μg/ml puromycin. The protein was purified by affinity chromatography using Ni-NTA agarose (Qiagen) followed by gel filtration chromatography, as previously described[56,57]. The peak fractions were pooled and concentrated to 10 mg/ml using a 10-kDa MWCO Millipore filter (MilliporeSigma).

Soluble CD4. Cells that express strep-tagged CD4 were grown in 250-ml roller bottles with DMEM containing 10% FBS and 1 μg/ml puromycin. Once the cells reached ~70% confluence, the medium was replaced with HEK293T serum-free expression medium. After 5 days, cell supernatants were collected and loaded onto a Strep-Tactin Sepharose (IBA Lifesciences) column. The column was then washed with 100 mM Tris-HCl, pH 8.0 and 150 mM NaCl. The protein was eluted with 100 mM Tris-HCl, pH 8.0, 150 mM NaCl and 2.5 mM desthiobiotin (IBA). Eluted fractions were analysed by sodium dodecyl sulfate–polyacrylamide gel electrophoresis (SDS–PAGE), and peak fractions containing CD4 were pooled and dialysed against 100 mM Tris-HCl, pH 8.0 and 150 mM NaCl using a dialysis tubing with 6–8 kDa MWCO (Spectrum Laboratories). The protein was further purified by gel filtration chromatography using a Superdex 200 column (GE Healthcare) in a buffer containing 30 mM Tris-HCl, pH 8.0 and 150 mM NaCl. The peak fractions were pooled and concentrated to 10 mg/ml using 10-kDa MWCO Millipore filters.

Anti-V3 antibody 447-52D. The hybridoma cells that express anti-V3 antibody 447-52D were grown in roller bottles with RPMI medium supplemented with ultra-low IgG FBS (Thermo Fisher Scientific). The antibody was purified by affinity chromatography using GammaBind Plus Sepharose (GE Healthcare) as previously described[57,58]. The eluted fractions were analysed by SDS–PAGE and those that contained the antibody were pooled, concentrated, frozen in liquid nitrogen and stored at −80 °C.

Western blot and flow cytometry. Western blot was performed using an anti-CCR5 antibody following a previously described protocol[24]. To test CCR5 cell-surface expression and its binding to gp120, flow cytometry was carried out as previously described[24,59]. In brief, CCR5 was detected by PE mouse antihuman CD195 (BD Biosciences) and bound-gp120 was stained with anti-His-tagged PE conjugated mouse IgG (R&D Systems). Extensive washing of the gp120-bound cells with PBS or leaving them in PBS up to 4 h did not change the fluorescence signals, suggesting that gp120 dissociates very slowly from CCR5 on the cell surfaces. Control experiments were carried out to ensure the binding specificity and all experiments were repeated at least three times with almost identical results.

CCR5 functional assays. When CCR5 is activated by its chemokine ligands, its intracellular regions can interact mainly with the inhibitory heterotrimeric G protein $G\alpha_i$; coupling of CCR5 to $G\alpha_i$ reduces the intracellular concentration of the secondary messenger cyclic AMP (cAMP)[60]. We measured changes in the intracellular cAMP concentration in these cells when CCR5 was activated by chemokine CCL5 using ACTOne technology[61] (Codex Biosolutions). In brief, HEK293T cells or CCR5-expressing cells were transfected with the pcDNA3.2-cyclic nucleotide-gated (CNG) channel gene using Lipofectamine 3000 reagent (Thermo Fisher Scientific). About 24 h after transfection, the cells were transferred to a 384-well black clear plate at a density of 1.2×10^4 cells/well in 20 μl culture medium. On day 3, the cells were treated with different concentrations of CCL5, CD4, gp120 or the gp120–CD4 complex in the presence of 25 μM 4-(3-butoxy-4-methoxybenzyl) imidazolidin-2-one (Ro20-1724)—a phosphodiesterase 4 inhibitor—and 500 nM 5′-N-ethylcarboxamidoadenosine (NECA), an endogenous adenosine A2b receptor agonist that increases cellular cAMP levels. Changes in the cAMP concentration in live cells directly correlate with the ion flux through CNG channel, which was measured by a fluorescent plate reader Hamamatsu FDSS 7000 after staining with the ACTOne membrane potential dye (Codex Biosolutions). Similar results were obtained for both the HEK293T-CCR5 and Expi293F-CCR5 stable cell lines.

It has previously been reported that HIV-1 gp120 or viral particles can induce CCR5 or CXCR4 cell signalling, measured as calcium flux in primary unstimulated $CD4^+$ T cells[62]. To test calcium flux in our HEK293T-CCR5 stable cells in response to gp120, we seeded the cells in a 384-well black clear plate at the density of 1.5×10^4 cells/well in 20 μl culture medium. On the second day, 20 μl of 1× Non-Wash Calcium Dye solution (Codex BioSolutions) was added to each well. The plate was then incubated in a CO_2 incubator at 37 °C for one hour. The different concentrations of various ligands were prepared in 1× Hank's balanced salt solution (HBSS) with 20 mM HEPES (pH 7.4) (at the 5× of the final concentration). The fluorescence intensity of each well was recorded on the FDSS 7000 reader at a rate of 1 image per second with an excitation wavelength of 480 nM and an emission wavelength of 540 nM. The base line of each well was recorded for 10 s before addition of 10 μl of a prepared ligand at 5× of the final concentration. Fluorescence intensity was recorded for additional 390 s.

Purification of the CD4–gp120–CCR5 complex. We first screened many gp120 proteins derived from different HIV-1 isolates for binding to the cell-surface-expressed CCR5 in the presence of soluble CD4 by flow cytometry and small-scale purification in detergent. The 92BR020 gp120 was chosen based on not only the stability of its CCR5 complex on the cell surfaces, but also the stability of the purified complex in detergent. For large-scale protein purification, we grew Expi293F stable cells stably transfected with the CCR5 expression construct in suspension. The cells were collected at the density of ~5–7 × 10^6/ml by centrifugation (4,000 r.p.m. at 4 °C for 30 min). The cell pellets were washed with PBS, re-suspended in PBS supplemented with 1% BSA, and incubated with the preformed CD4–gp120 complex for one and half hours at 4 °C. The cells were then washed three times with PBS, resuspended in a lysis buffer containing100 mM Tris-HCl, pH 8.0, 150 mM NaCl, 1 mM EDTA, 1% lauryl maltose neopentyl glycol (w/v) (LMNG, Anatrace), 0.2% cholesteryl hemisuccinate (w/v) (CHS, Anatrace), EDTA-free complete protease inhibitor cocktail (Roche), and incubated at 4 °C for one hour. The supernatants were collected after centrifugation (18,000 r.p.m. at 4 °C for 60 min), and then loaded on a strep-tactin column equilibrated with the lysis buffer. The column was washed with 5 column volumes of a washing buffer (100 mM Tris-HCl, pH 8.0, 150 mM NaCl, 1 mM EDTA, 0.5% LMNG (w/v), 0.04% CHS (w/v)), followed by 50 column volumes of another washing buffer (100 mM Tris-HCl, pH 8.0, 150 mM NaCl, 1 mM EDTA, 0.001% LMNG (w/v), 0.1% *n*-dodecyl-β-D-maltopyranoside (DDM, Anatrace) (w/v), 0.04% CHS (w/v)). The CCR5 complex was eluted by an elution buffer containing 100 mM Tris-HCl, pH 8.0, 150 mM NaCl, 1 mM EDTA, 0.001% LMNG (w/v), 0.1% DDM (w/v), 0.04% CHS (w/v), and 5 mM desthiobiotin. Elution fractions were analysed by SDS–PAGE and those that contained the CCR5 complex were pooled.

The anti-V3 antibody 447-52D binds only the CD4–gp120 complex with the V3 loop exposed, and not the CD4–gp120–CCR5 complex with the V3 region protected by possible interactions with the coreceptor. To remove extra CD4–gp120 complex, 447-52D was loaded onto the GammaBind Plus column, which was subsequently washed with 50 column volumes of PBS to remove unbound antibody. The column was then equilibrated with the elution buffer for the strep-tactin column. The pooled fractions containing the CCR5 complex from the strep-tag purification were loaded onto the 447-52D column. The flow-through was collected and then concentrated using an Amicon Ultra Centrifugal Filter (MWCO 100 kDa). The complex was further purified by size-exclusion chromatography on a Sepharose 6 10/300 column (GE Healthcare) in a buffer containing 100 mM Tris-HCl, pH 8.0, 150 mM NaCl, 1 mM EDTA, 0.001% LMNG (w/v), 0.025% DDM (w/v) and 0.04% CHS (w/v). Eluted fractions containing the CCR5 complex were pooled and concentrated. The complex could be concentrated to at least 3 mg/ml without any aggregation on a size-exclusion column.

Negative-stain electron microscopy. To prepare grids, 2.5 μl of the freshly purified CCR5 complex was adsorbed to a glow-discharged carbon-coated copper grid, washed with deionized water, and stained with freshly prepared 0.75% uranyl formate. Images were recorded at room temperature with a magnification of 52,000× and a defocus value of 1.5 μm following low-dose procedures, using a Philips Tecnai F20 electron microscope (Thermo Fisher Scientific) equipped with a Gatan US4000 CCD camera and operated at a voltage of 200 kV. Particles were

picked manually and 2D class averages were generated by using EMAN2 software package[63]. These 2D averages were used to generate a 3D initial model starting from a density of isotropic Gaussian distribution[64].

Cryo-EM sample preparation and data collection. To prepare cryo grids, 3 μl of the freshly purified CD4–gp120–CCR5 complex at 1.0 mg/ml was applied to a 1.2/1.3 Quantifoil grid (Quantifoil Micro Tools GmbH), which had been glow-discharged for 90 s at 20 mA. Grids were immediately plunge-frozen in liquid ethane using a Vitrobot (Thermo Fisher Scientific) with a blotting time of 4 s. The grids were first screened for ice thickness and particle distribution using a Talos Arctica transmission electron microscope (Thermo Fisher Scientific) operated at 200 kV and equipped with a K2 Summit direct detector (Gatan). For data collection, images were acquired with selected grids using a Titan Krios transmission electron microscope (Thermo Fisher Scientific) operated at 300 kV with a K2 detector. Automated data collection was carried out using SerialEM[65] at a magnification of 130,000× and the K2 detector in super-resolution mode (pixel size, 0.529 Å) at a dose rate of ~6 electrons per physical pixels per second. Each movie had a total accumulated exposure of ~46 e/Å^2 fractionated in 35 frames of 200 ms. Total of four datasets were acquired in different sessions using a defocus range of 1.0–2.8 μm.

Image processing and 3D reconstructions. For cryo-EM data, drift correction was performed using MotionCor2[66] and images were binned 2 × 2 by Fourier cropping to a pixel size of 1.059 Å. The contrast transfer function was estimated by CTFFIND4[67] using motion-corrected sums without dose-weighting. Motion-corrected sums with dose-weighting were used for all other image processing. RELION 2.1[26] was used for particle picking, 2D classification, 3D classification and refinement procedures. Around 2,000 particles were manually picked and classified by 2D classification to generate the templates for automatic particle picking. After the manual inspection of auto-picked particles, a total of 1,707,675 particles were extracted from 9,776 selected images (out of 10,530 movie stacks in total collected in four sessions). These particles were subjected to 2D classification in three groups, giving a total of 1,546,032 particles. The low-resolution negative-stain reconstruction of the complex was low-pass-filtered to a 60 Å resolution, and used as the initial model for 3D classification. A total of 691,508 particles from 3D classes that show clear structural features were combined and subjected to 3D refinement, which led to a reconstruction at 4.6 Å resolution. Local refinement with a mask to exclude the last two domains (D3–D4) of CD4 improved the overall resolution to 4.0 Å. Cryo-EM particles were then subjected to 3D classification with signal subtraction, focusing on gp120, the first domain of CD4 and half of the CCR5. The best class with the highest resolution contained 307,346 particles and 3D refinement produced a map at 4.5 Å resolution. Further local refinement using a mask to exclude the last two domains of CD4 led to a final map at 3.9 Å resolution.

Reported resolutions are based on the gold-standard Fourier shell correlation using the 0.143 criterion, calculated with SAMUEL ('Simplified Application Managing Utilities for EM Labs') scripts of the Liao laboratory (https://liao.hms.harvard.edu/samuel). All density maps were corrected for the modulation transfer function of the K2 summit direct detector and then sharpened by applying a temperature factor that was estimated using post-processing in RELION. Local resolution was determined using LocalRes in RELION with half-reconstructions as input maps.

Model building. The initial model of gp120 was a homology model calculated by I-TASSER[68], using the cryo-EM structure of gp120 from the CD4-bound SOSIP trimer (PDB ID: 5VN3) as a template. The crystal structures of CD4 (PDB ID: 1WIO) and CCR5 (PDB ID: 5WIU) were also used as initial templates for model building. Several rounds of manual building were performed in Coot[69]. The model was finalized by refinement in Phenix[70] against the 3.9 Å cryo-EM map. The refinement statistics are summarized in Extended Data Table 1.

Reporting summary. Further information on research design is available in the Nature Research Reporting Summary linked to this paper.

Data availability

The atomic structure coordinates are deposited in the RCSB Protein Data Bank (PDB) under the accession numbers 6MEO and 6MET; and the electron microscopy maps have been deposited in the Electron Microscopy Data Bank (EMDB) under the accession numbers EMD-9108 and EMD-9109. All other related data generated during and/or analysed during the current study are available from the corresponding author on reasonable request.

71. Feng, Y., Broder, C. C., Kennedy, P. E. & Berger, E. A. HIV-1 entry cofactor: functional cDNA cloning of a seven-transmembrane, G protein-coupled receptor. *Science* **272**, 872–877 (1996).
72. Wu, L. et al. CD4-induced interaction of primary HIV-1 gp120 glycoproteins with the chemokine receptor CCR-5. *Nature* **384**, 179–183 (1996).
73. Alkhatib, G. et al. CC CKR5: a RANTES, MIP-1α, MIP-1β receptor as a fusion cofactor for macrophage-tropic HIV-1. *Science* **272**, 1955–1958 (1996).
74. Choe, H. et al. The β-chemokine receptors CCR3 and CCR5 facilitate infection by primary HIV-1 isolates. *Cell* **85**, 1135–1148 (1996).
75. Deng, H. et al. Identification of a major co-receptor for primary isolates of HIV-1. *Nature* **381**, 661–666 (1996).
76. Doranz, B. J. et al. A dual-tropic primary HIV-1 isolate that uses fusin and the β-chemokine receptors CKR-5, CKR-3, and CKR-2b as fusion cofactors. *Cell* **85**, 1149–1158 (1996).
77. Dragic, T. et al. HIV-1 entry into CD4$^+$ cells is mediated by the chemokine receptor CC-CKR-5. *Nature* **381**, 667–673 (1996).
78. Jin, J. et al. CCR5 adopts three homodimeric conformations that control cell surface delivery. *Sci. Signal.* **11**, eaal2869 (2018).

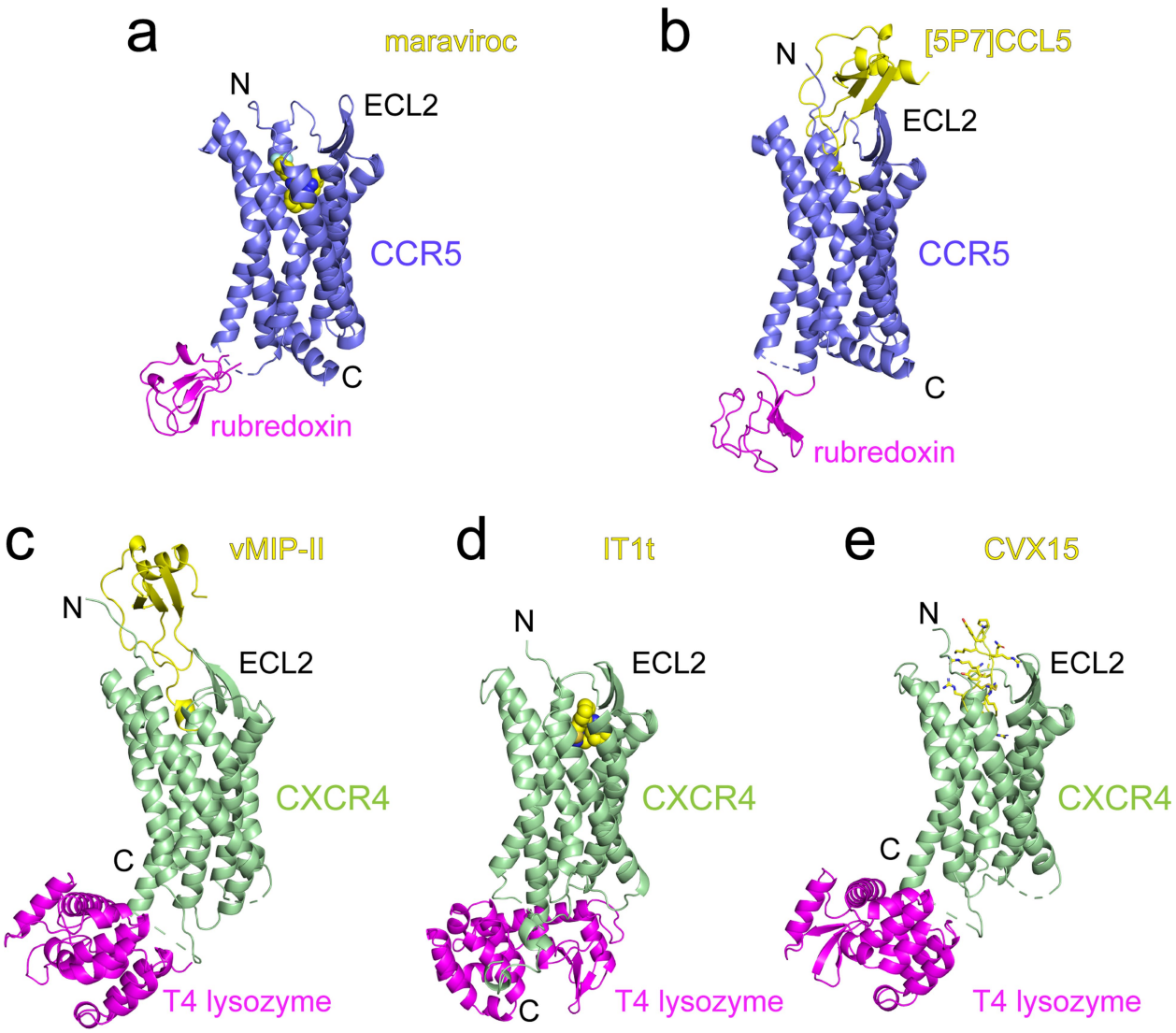

Extended Data Fig. 1 | Previously known structures of CCR5 and CXCR4. CCR5 and CXCR4 were identified as the coreceptors for HIV-1 entry in 1996[71–77]. **a**, **b**, Crystal structures of a modified CCR5 (C224–N226 deleted and replaced with rubredoxin; ΔF320–L352; and the point mutations C58Y, G163N, A233D and K303E) in complex with the HIV entry-inhibitor maraviroc (PDB ID: 4MBS[7]) (**a**) and a modified chemokine [5P7]CCL5 (an antagonist; PDB ID: 5UIW[10]) (**b**). CCR5 is shown in ribbon diagram in blue, with the internally fused rubredoxin in magenta and the ligands in yellow. **c**–**e**, Crystal structures of an engineered CXCR4 in complex with a viral chemokine antagonist vMIP-II (PDB ID: 4RWS[15]) (**c**), a small molecule antagonist IT1t (PDB ID: 3ODU[14]) (**d**) and a cyclic peptide antagonist CVX15 (PDB ID: 3OE0[14]) (**e**). CXCR4 is shown in green, the fused T4 lysozyme in magenta and the ligands in yellow.

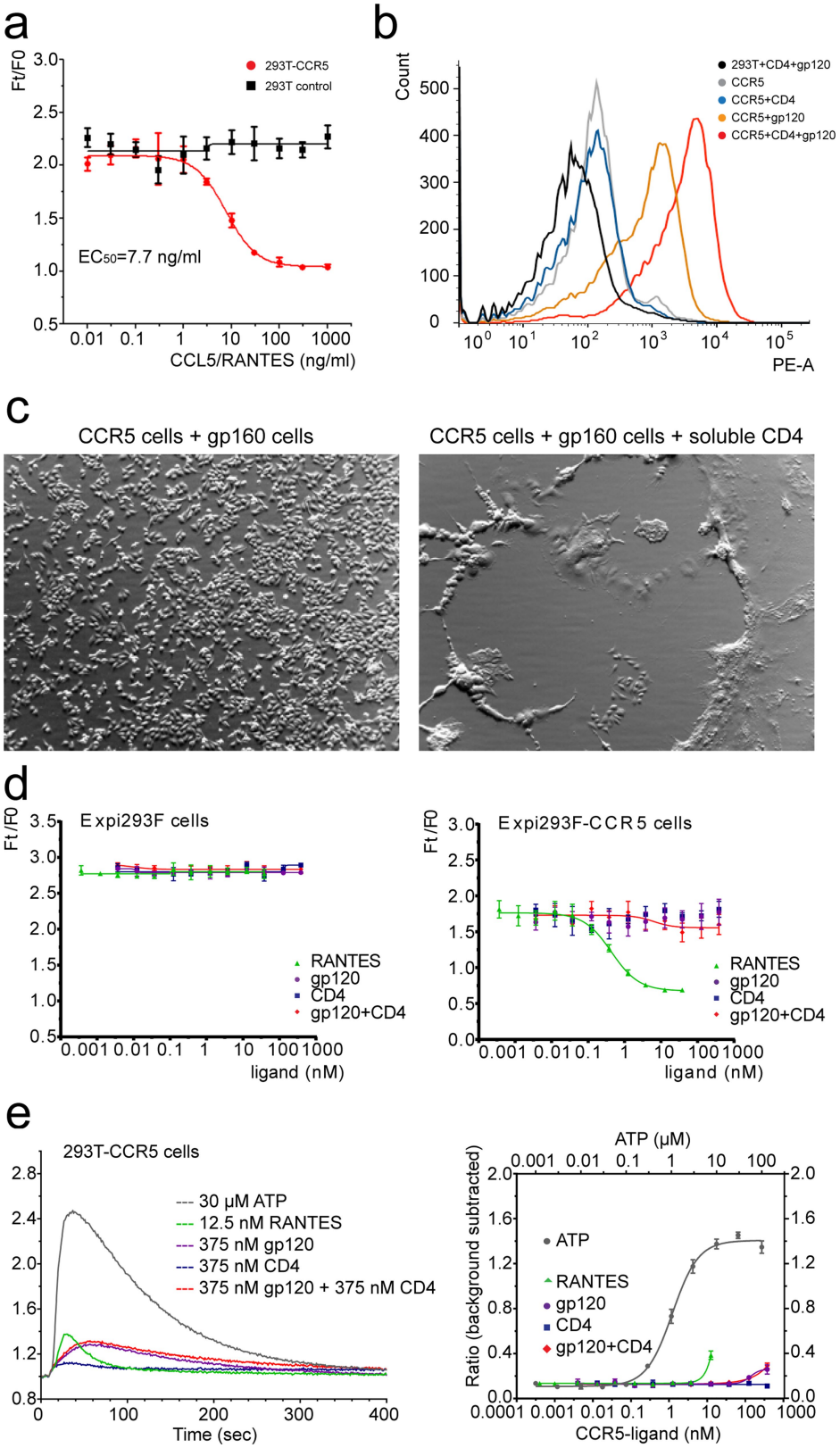

Extended Data Fig. 2 | See next page for caption.

Extended Data Fig. 2 | Characterization of stable cell lines (HEK293T and Expi293F) expressing wild-type human CCR5. a, Chemokine receptor assay. HEK293T and HEK293T-CCR5 (stable) cells were treated with different concentrations of CCL5. F_t/F_0 is a fluorescence-signal ratio proportional to that of intracellular cAMP concentration at 40 min after CCL5 activation and at time 0. The dose–response curves were plotted for both HEK293T (black) and HEK293T-CCR5 (red) cells. The experiment was carried out in quadruplicate, and repeated at least three times with similar results. Error bars indicate the standard deviation calculated by the STDEV function in Excel. **b**, Flow cytometry histograms of HIV-1 gp120 binding to CCR5 expressed on the cell surfaces in the absence (orange) or presence (red) of soluble CD4. HEK293T cells (black), CCR5-expressing cells only (grey) and CCR5-expressing cells with soluble CD4 only (blue) were negative controls. The experiment was repeated independently at least twice with similar results. **c**, HIV-1 Env-mediated cell–cell fusion. HEK293T cells stably transfected with CCR5 were mixed with HIV-1 Env (gp160)-expressing cells in the absence or presence of soluble CD4. The CCR5 cells fuse with CD4-triggered Env cells very efficiently, and form large syncytia that cover almost the entire well. The experiment was repeated independently twice with similar results. **d**, Chemokine receptor assay by various ligands. As in **a**, Expi293F and Expi293F-CCR5 (stable) cells were treated with CCL5, gp120, CD4 or the complex of gp120 and CD4. The dose–response curves were plotted for both Expi293F as a control (left) and Expi293F-CCR5 (right) cells, with different ligands as indicated. The experiment was carried out in quadruplicate and repeated at least three times with similar results. Error bars indicate the standard deviation calculated by the STDEV function in Excel. **e**, Left, kinetic curves of 5 representative wells of HEK293T-CCR5 cells treated with 5 different ligands as indicated. ATP activates the endogenous G_q-coupled G-protein-coupled receptor (P2Y receptor), as a positive control. The ratio represents fluorescence intensity divided by baseline intensity. Right, dose–response curve of each ligand. The *y* axis is a background-subtracted ratio (peak fluorescent intensity ratio − 1). We conclude that our gp120 and gp120–CD4 do not activate G-protein-mediated calcium flux at the concentrations tested here. The experiment was carried out in quadruplicate and repeated twice with similar results. Error bars indicate the standard deviation calculated by the STDEV function in Excel.

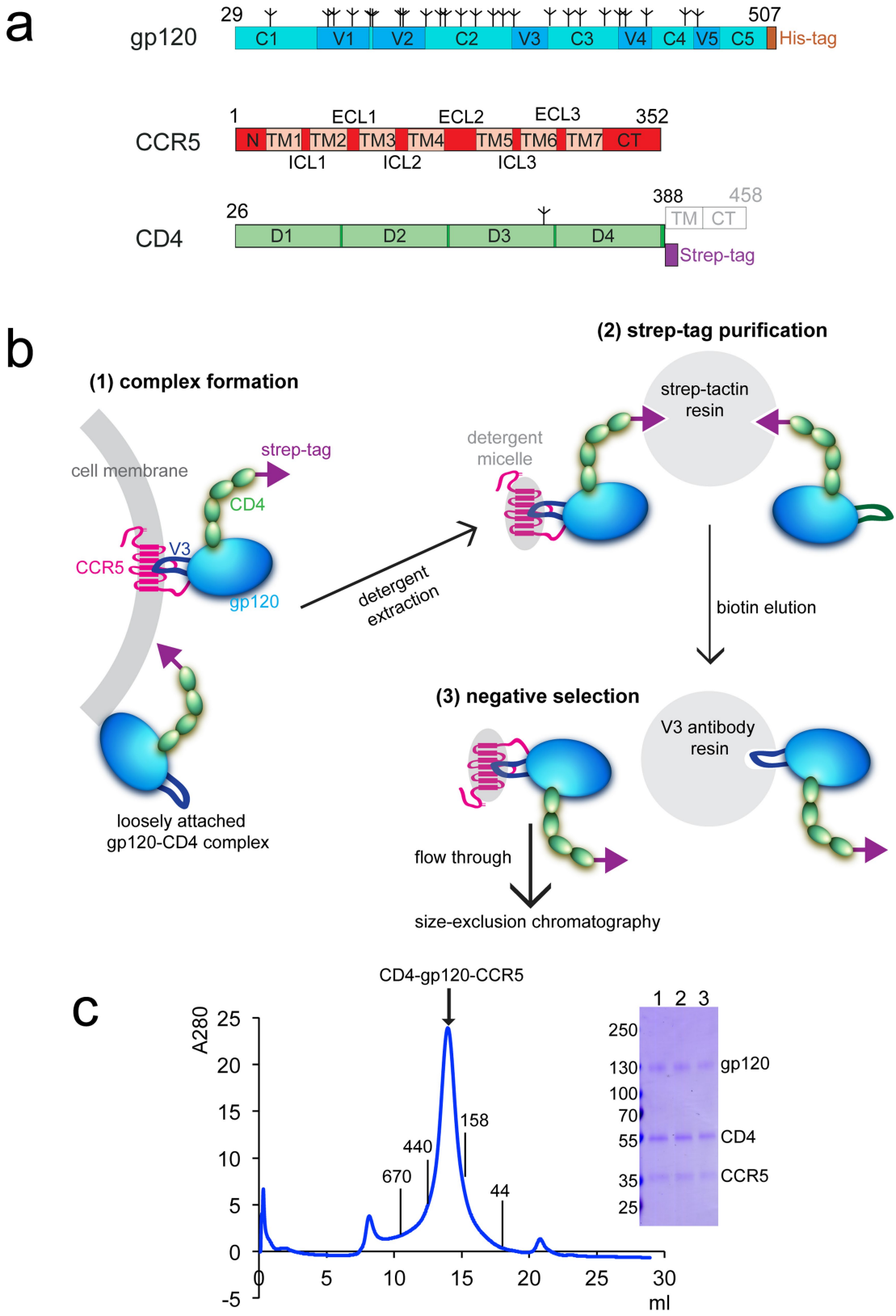

Extended Data Fig. 3 | See next page for caption.

Extended Data Fig. 3 | Purification of the CD4-gp120-CCR5 complex. **a**, Schematic of expression constructs for HIV-1 gp120, human CCR5 and CD4. Segments of gp120 are designated as follows: C1–C5, conserved regions 1–5; V1–V5, variable regions 1–5; and His-tag, a six-histidine tag. Tree-like symbols represent glycans. Abbreviations used for segments of CCR5 are: N, N terminus; TM1–TM7, transmembrane helices 1–7; ECL1–ECL3, extracellular loops 1–3; ICL1–ICL3, intracellular loops 1–3; and CT, cytoplasmic tail. For CD4, the following abbreviations are used: D1–D4, immunoglobulin (Ig) domains 1–4; and strep tag, a purification tag. The transmembrane segment (TM) and cytoplasmic tail (CT) in grey are truncated in the expression construct. **b**, Unmodified human CCR5 in complex with HIV-1 gp120 and four-domain CD4 was purified by the following steps. (1) Complex formation: HIV-1 gp120 (light blue) and strep-tagged, four-domain CD4 (green) were incubated with CCR5 (magenta)-expressing cells to allow formation of the CD4–gp120–CCR5 complex on cell surfaces. (2) Strep-tag purification: the CCR5 complex and some of the CD4–gp120 complex were captured to strep-tactin resin via the strep-tagged CD4 (strep tag in purple). They were eluted by D-desthiobiotin under mild conditions. (3) Negative selection by an anti-V3 antibody to remove the CD4–gp120 complex. The CCR5 complex was further purified by size-exclusion chromatography. **c**, The purified CD4–gp120–CCR5 complex was resolved by gel-filtration chromatography on a Superose 6 column in the presence of the detergent LMNG. The molecular-mass standards include thyoglobulin (670 kDa), ferritin (440 kDa), γ-globulin (158 kDa) and ovalbumin (44 kDa). The expected size of the CCR5 complex is ~310 kDa (120 kDa for gp120, 50 kDa for four-domain CD4, 40 kDa for CCR5 and ~100 kDa for LMNG micelle). Peak fractions were analysed by Coomassie-stained SDS–PAGE (lanes 1–3). Labelled bands were confirmed by western blot and protein sequencing. The experiment was repeated independently at least 15 times with similar results.

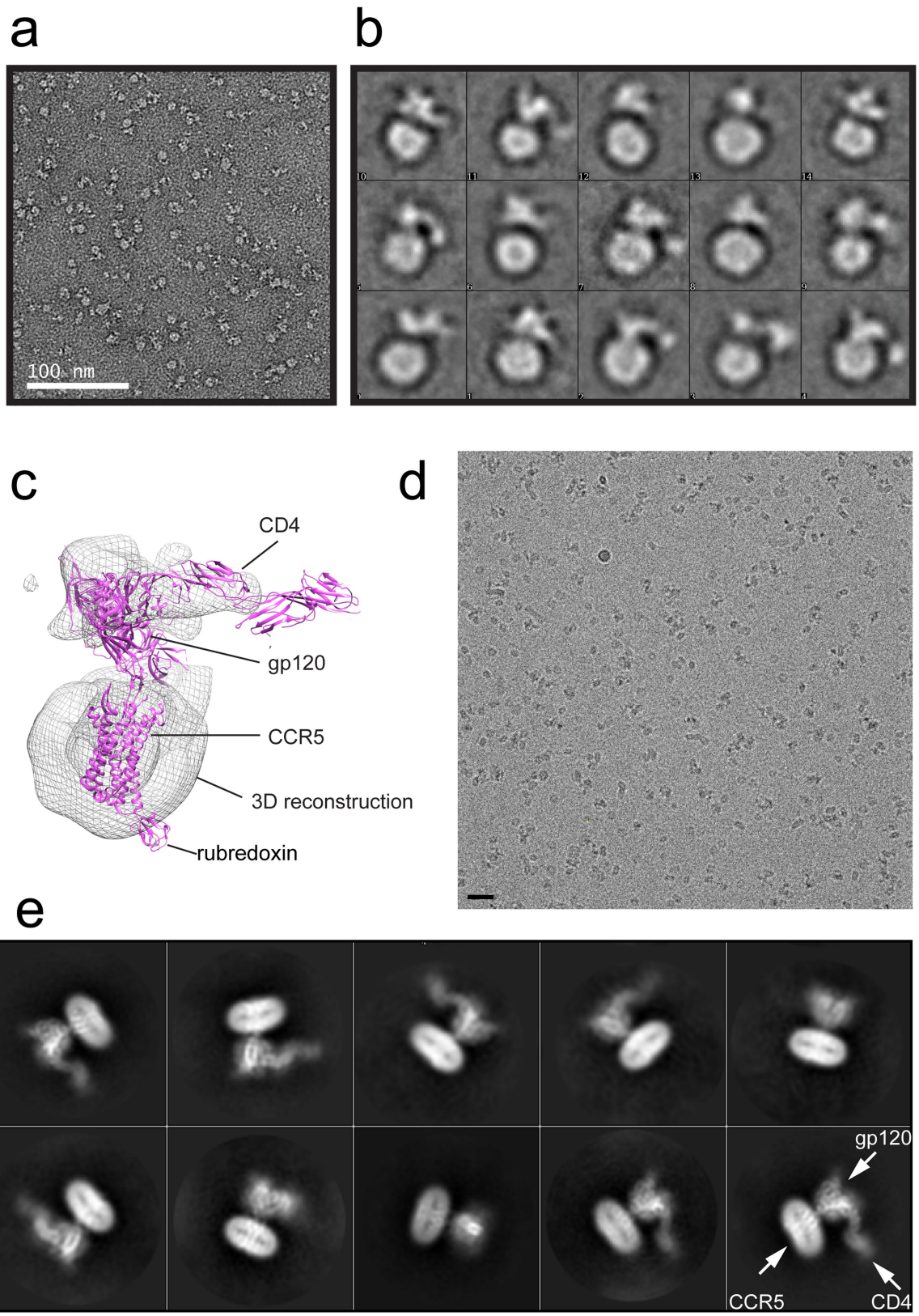

Extended Data Fig. 4 | Characterization of the CD4–gp120–CCR5 complex by electron microscopy. a, Representative image of the CD4–gp120–CCR5 complex in negative stain. The experiment was repeated independently at least 4 times with similar results. **b**, 2D averages of the negatively stained CD4–gp120–CCR5 complex. The box size of 2D averages is ~330 Å. **c**, 3D reconstruction of the negatively stained CD4–gp120–CCR5 complex, fitted with a gp120 structure containing an extended V3 loop (PDB ID: 2QAD[20]), four-domain CD4 (PDB ID: 1WIO) and CCR5 (PDB ID: 4MBS). **d**, A representative cryo-EM image of the four-domain-CD4–gp120–CCR5 complex. Scale bar, 25 nm. Five independent large datasets were collected with similar results. **e**, 2D averages of the cryo-EM particle images show secondary structural features for both gp120 and CCR5.

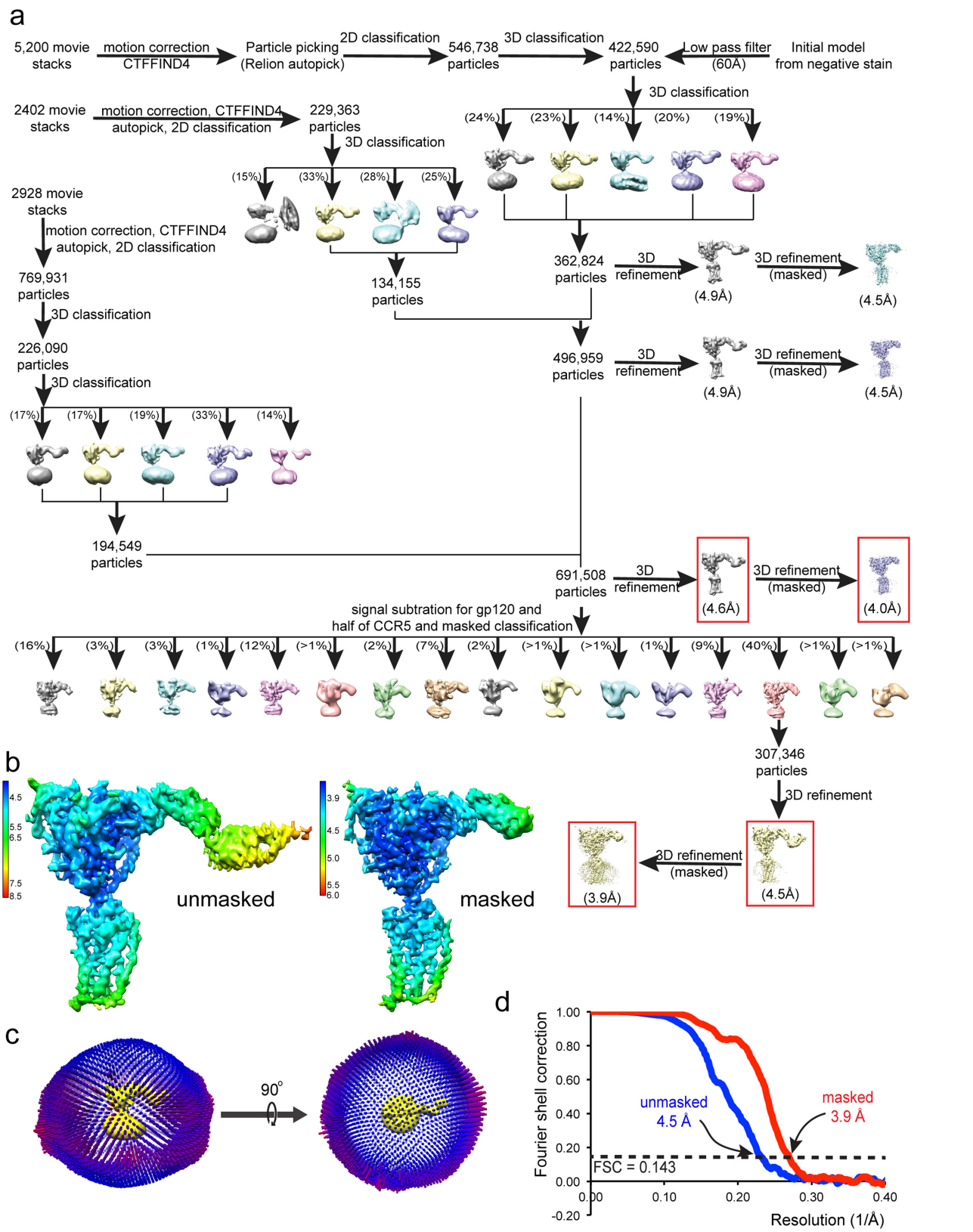

Extended Data Fig. 5 | Single-particle cryo-EM analysis of the CD4–gp120–CCR5 complex. a, Data-processing workflow for the CD4–gp120–CCR5 complex. **b**, 3D reconstructions of the CD4–gp120–CCR5 complex refined with no mask at an overall resolution of 4.5 Å (left), and with a mask to exclude the last two domains of CD4 at a resolution of 3.9 Å (right), are coloured according to local resolution estimated by RELION. **c**, The angular distribution of the cryo-EM particles used in the reconstruction is also shown in respect to both the side and top views of the electron microscopy map. **d**, Gold standard Fourier shell correlation curves of the unmasked and masked electron microscopy reconstructions shown in **b**.

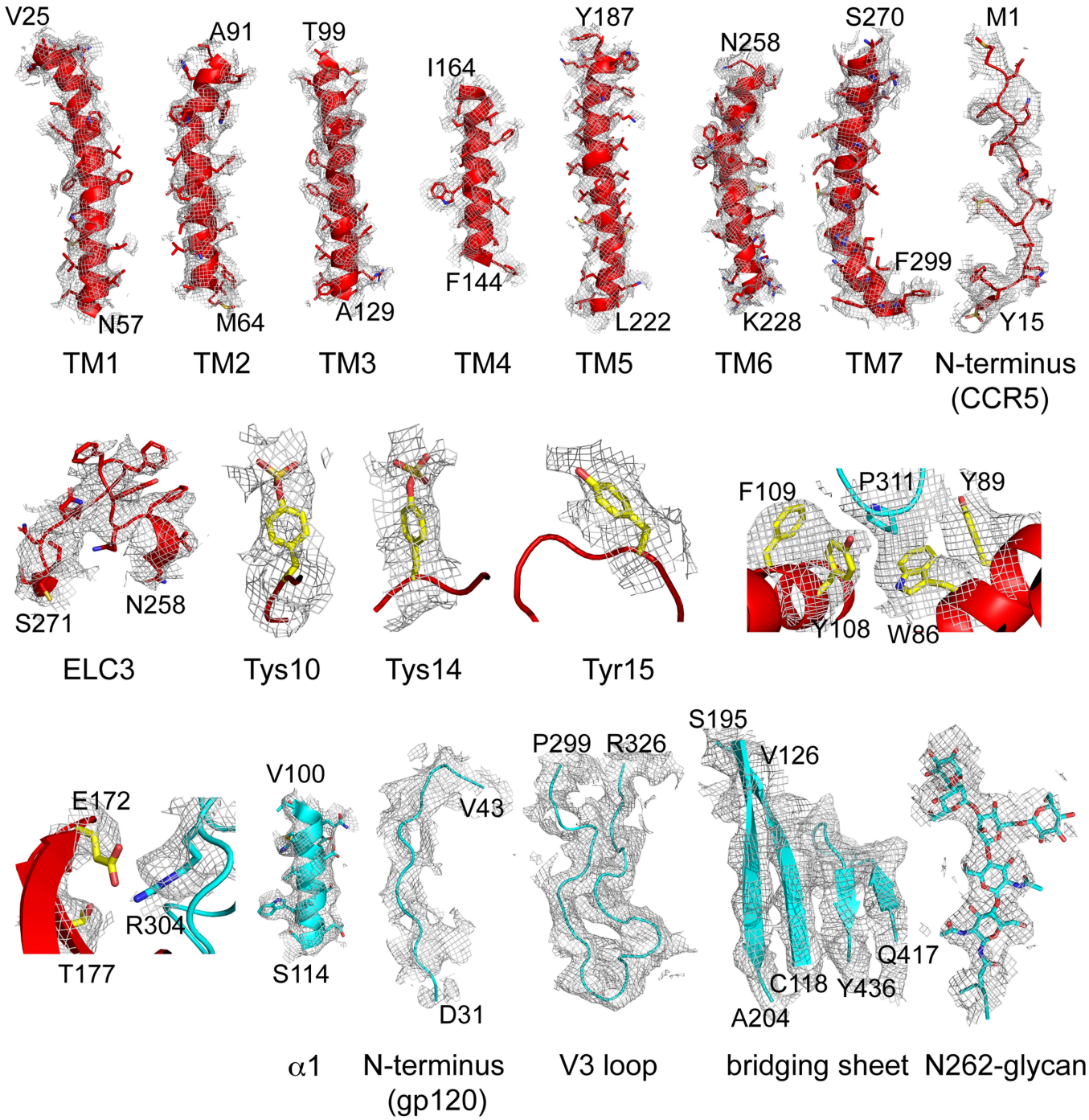

Extended Data Fig. 6 | Gallery of representative density for the CD4–gp120–CCR5 complex. Representative density in grey mesh from the 3.9 Å resolution electron microscopy map is shown for transmembrane helices TM1–TM7, the N terminus of CCR5, extracellular loop 3 (ELC3) near TM6, Tys10, Tys14 and Tyr15 (red model); two V3 regions; and for helix α1, N terminus, V3 loop, the bridging sheet and *N*-linked glycan at N262 of gp120 (cyan model).

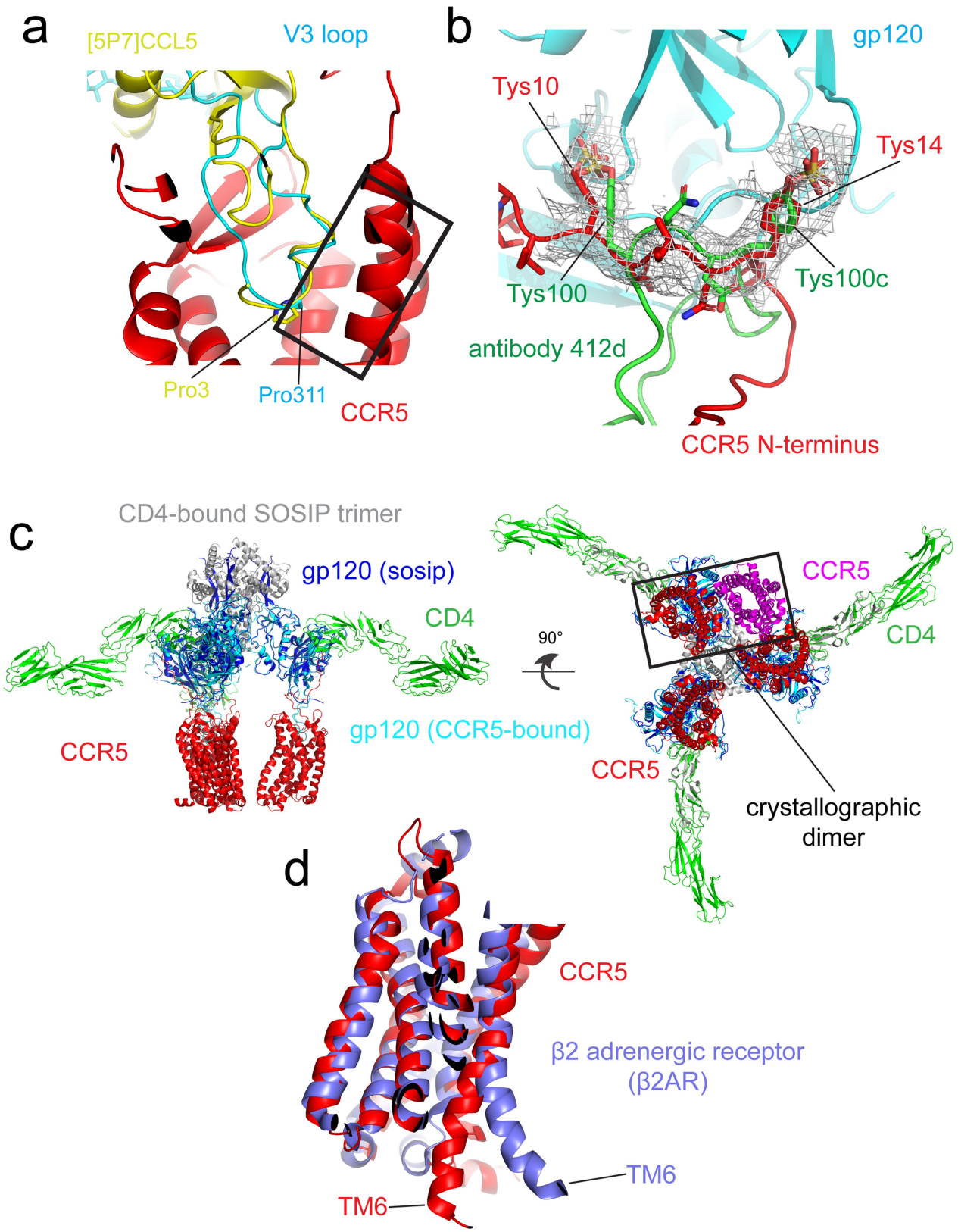

Extended Data Fig. 7 | See next page for caption.

Extended Data Fig. 7 | Comparison of the conformations of the V3 loop and [5P7]CCL5 in complex with CCR5, as well as of gp120-bound CCR5 and G-protein-bound β_2 adrenergic receptor. a, The structures of the CD4–gp120–CCR5 and [5P7]CCL5–CCR5 complexes are superposed on CCR5 (red). The V3 loop of gp120 with its Pro311 in stick model is in cyan and [5P7]CCL5 with its Pro3 in stick model in yellow. Residues 309–316 of the V3 loop and residues 1–8 of [5P7]CCL5 adopt a very similar structure, and are highlighted in a rectangular box. **b**, Superposition of the structures of the N terminus of the gp120-bound CCR5 (red) and the complementarity-determining region H3 loop of antibody 412d in complex with gp120 core (green). The electron microscopy density of the CD4–gp120–CCR5 complex is shown in grey. The positions of the sulfated tyrosine ('Tys') residues, including Tys10 and Tys14 (from CCR5) and Tys100 and Tys100c (from 412d), are indicated. **c**, A model for interactions of three CD4 receptors and three CCR5 coreceptors with the SOSIP Env trimer. The side and bottom views of a composite structure of the CD4–CCR5–SOSIP Env trimer complex are shown. The model was generated using the CD4-bound SOSIP trimer (PDB ID: 5VN3) and the structure of the CD4–gp120–CCR5 complex from this study. All the structures were aligned on the basis of the core region of gp120. CCR5 is shown in red, CD4 in green, gp120 in blue, the gp120 of SOSIP in dark blue and the gp41 of SOSIP in grey. The crystallographic dimer of CCR5 (PDB ID: 4MBS) is also shown, on the left only, in a rectangular box. The observed crystallographic dimer of CCR5 or the transmembrane helix 5-mediated dimer by modelling does not seem to be relevant to binding to either monomeric or trimeric gp120[7,78]. **d**, Superposition of the structures of the gp120-bound CCR5 (red) and the G_s-protein-bound β_2 adrenergic receptor (blue). The position of TM6, which is critical for the activation of G-protein-coupled receptors, is indicated.

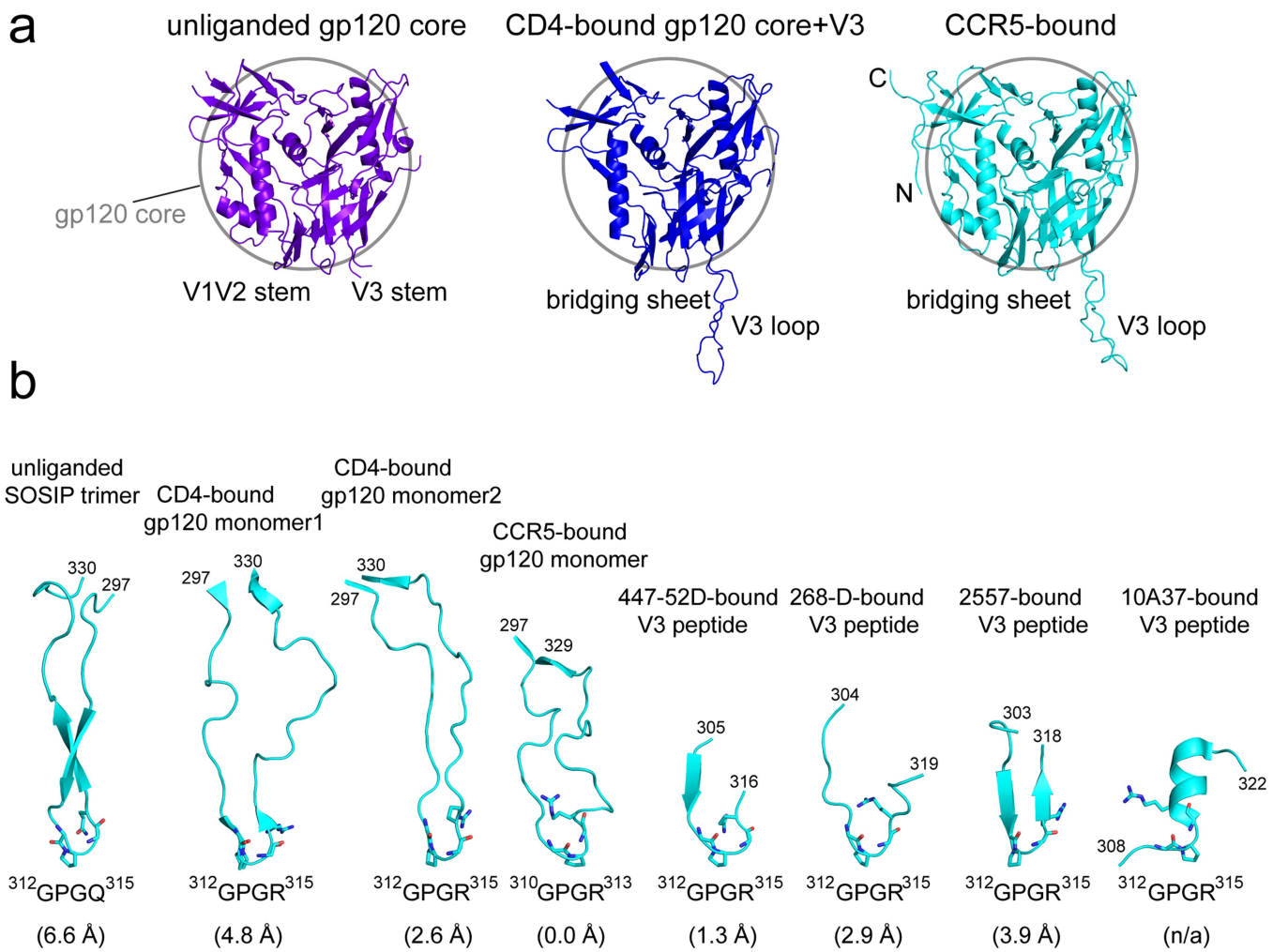

Extended Data Fig. 8 | Comparison of conformations of different structures of monomeric gp120 and various V3 loops. a, Comparison of structures of an unliganded gp120 core (PDB ID:4OLV; purple), a CD4-bound monomeric gp120 core with the V3 loop (PDB ID: 2QAD; blue) and gp120 in complex with CD4 and CCR5 from this study (cyan). The gp120 core region is marked by a circle with a diameter of 50 Å. The N and C termini, V1V2 stem, V3 stem or loop and bridging sheet are indicated. **b**, Representative conformations that an HIV-1 V3 loop can adopt. From left to right, V3 loop in the unliganded SOSIP BG505 Env trimer (PDB ID: 4ZMJ); the first-V3-containing gp120 core in complex with CD4 and antibody X5 (PDB ID: 2B4C[29]); CD4- and 412d-bound monomeric gp120 core with V3 (PDB ID: 2QAD); CCR5-bound intact gp120 (this study); and V3 peptide in complex with antibody 447-52D (PDB ID: 3GHB[36]); antibody 268-D (PDB ID: 3GO1[37]); antibody 2557 (PDB ID: 3MLV[37]); and antibody 10A37 (PDB ID: 5V6L[38]). The root-mean-square deviation of each structure (except for 5V6L), relative to the CCR5-bound gp120 monomer, is shown at the bottom in parentheses.

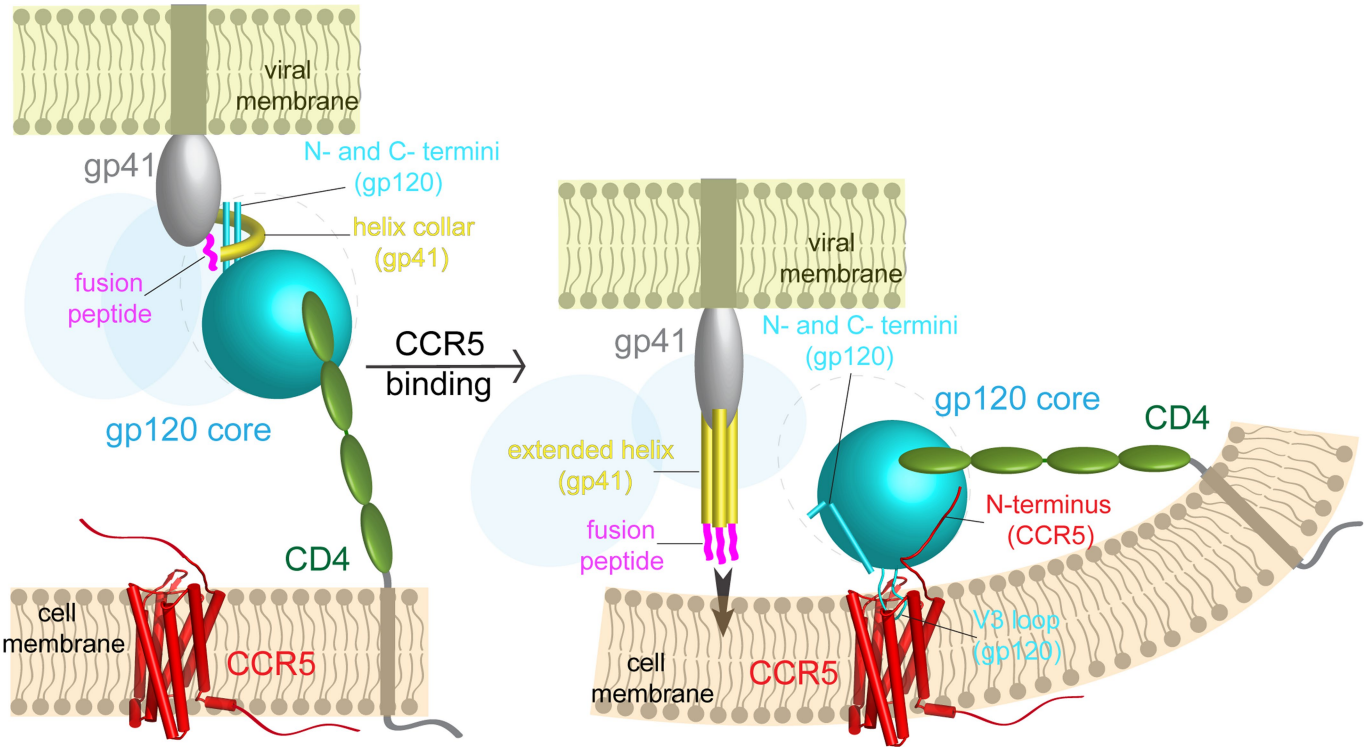

Extended Data Fig. 9 | Model of HIV-1 Env activation to induce membrane fusion. A hypothesis of how the cellular receptors CD4 and CCR5 trigger the HIV-1 Env trimer to induce membrane fusion and viral entry. Left, virus attaches to the target cell by gp120 (cyan) binding to CD4 (green). Helix collar (gp41), the four-helix collar gripping the N- and C termini of gp120. Right, immediate binding by CCR5 (red) prevents rapid dissociation between gp120 and CD4, stabilizes the CD4-induced conformational changes within the Env trimer and brings the trimer close to the cell membrane. Simultaneous binding of gp120 to both CD4 and CCR5 may require bending in the cell membrane. The fusion peptide (magenta) of gp41 (grey) flips out owing to intrinsic conformational dynamics, which enables the bending back of the N and C termini of gp120. This bending blocks the fusion peptide from resuming its original position in the trimer. The movements of the fusion peptide and gp120 termini effectively weaken the non-covalent association between the two subunits and may lead to partial or complete dissociation of gp120, as well as a series of refolding events in gp41 to adopt the pre-hairpin intermediate conformation (with the fusion peptides inserting into the target-cell membrane). Extended helix (gp41), three helices in the fusion-intermediate conformation of gp41.

Extended Data Table 1 | Cryo-EM data collection, refinement and validation statistics

	CD4-gp120-CCR5 complex masked (EMDB -9108) (PDB 6MEO)	CD4-gp120-CCR5 complex overall (EMDB -9109) (PDB 6MET)
Data collection and processing		
Magnification	130000	130000
Voltage (kV)	300	300
Electron exposure (e–/Å^2)	~46	~46
Defocus range (μm)	1-2.8	1-2.8
Pixel size (Å)	0.529	0.529
Symmetry imposed	C1	C1
Initial particle images (no.)	1,707,575	1,707,575
Final particle images (no.)	307346	307346
Map resolution (Å)	3.9	4.5
FSC threshold	0.143	0.143
Refinement		
Initial model used (PDB code)	5UIW, 1WIO, 2QAD and 5VN3	5UIW, 1WIO, 2QAD and 5VN3
Map sharpening *B* factor (Å^2)	-190	-190
Model composition		
Non-hydrogen atoms	7462	8911
Protein residues	887	1074
Ligands	32	32
R.m.s. deviations		
Bond lengths (Å)	0.004	0.009
Bond angles (°)	0.954	1.386
Validation		
MolProbity score	1.60	1.97
Clashscore	3.51	5.84
Poor rotamers (%)	0.25	1.48
Ramachandran plot		
Favored (%)	92.77	90.83
Allowed (%)	7.23	8.51
Disallowed (%)	0	0.66

nature research

Corresponding author(s): Bing Chen

Reporting Summary

Nature Research wishes to improve the reproducibility of the work that we publish. This form provides structure for consistency and transparency in reporting. For further information on Nature Research policies, see Authors & Referees and the Editorial Policy Checklist.

Statistical parameters

When statistical analyses are reported, confirm that the following items are present in the relevant location (e.g. figure legend, table legend, main text, or Methods section).

n/a	Confirmed	
☐	☒	The exact sample size (*n*) for each experimental group/condition, given as a discrete number and unit of measurement
☐	☒	An indication of whether measurements were taken from distinct samples or whether the same sample was measured repeatedly
☒	☐	The statistical test(s) used AND whether they are one- or two-sided *Only common tests should be described solely by name; describe more complex techniques in the Methods section.*
☒	☐	A description of all covariates tested
☒	☐	A description of any assumptions or corrections, such as tests of normality and adjustment for multiple comparisons
☒	☐	A full description of the statistics including central tendency (e.g. means) or other basic estimates (e.g. regression coefficient) AND variation (e.g. standard deviation) or associated estimates of uncertainty (e.g. confidence intervals)
☒	☐	For null hypothesis testing, the test statistic (e.g. *F*, *t*, *r*) with confidence intervals, effect sizes, degrees of freedom and *P* value noted *Give P values as exact values whenever suitable.*
☒	☐	For Bayesian analysis, information on the choice of priors and Markov chain Monte Carlo settings
☒	☐	For hierarchical and complex designs, identification of the appropriate level for tests and full reporting of outcomes
☒	☐	Estimates of effect sizes (e.g. Cohen's *d*, Pearson's *r*), indicating how they were calculated
☐	☒	Clearly defined error bars *State explicitly what error bars represent (e.g. SD, SE, CI)*

Our web collection on statistics for biologists may be useful.

Software and code

Policy information about availability of computer code

Data collection	SerialEM (3.5)
Data analysis	FlowJo (10.5.3), EMAN2 (2.2), MotionCor2 (1.0.2), CTFFIND4 (4.1.5), RELION (2.1), I-TASSER, SAMUEL (17.05), Coot (0.8.8), Chimera (1.12), Phenix (1.11.1-2575).

For manuscripts utilizing custom algorithms or software that are central to the research but not yet described in published literature, software must be made available to editors/reviewers upon request. We strongly encourage code deposition in a community repository (e.g. GitHub). See the Nature Research guidelines for submitting code & software for further information.

Data

Policy information about availability of data

All manuscripts must include a data availability statement. This statement should provide the following information, where applicable:

- Accession codes, unique identifiers, or web links for publicly available datasets
- A list of figures that have associated raw data
- A description of any restrictions on data availability

The atomic structure coordinates are deposited in the Protein Data Bank under the accession number 6MEO and 6MET; and the EM maps in the EMDataBank

under the accession number EMD-9108 and EMD-9109. All other related data generated during and/or analyzed during the current study are available from the corresponding author on reasonable request.

Field-specific reporting

Please select the best fit for your research. If you are not sure, read the appropriate sections before making your selection.

☒ Life sciences ☐ Behavioural & social sciences ☐ Ecological, evolutionary & environmental sciences

For a reference copy of the document with all sections, see nature.com/authors/policies/ReportingSummary-flat.pdf

Life sciences study design

All studies must disclose on these points even when the disclosure is negative.

Sample size	Statistical methods were not needed to predetermine sample size for the biochemical and structural studies in this work. Multiple independent EM data sets were collected for structural analysis. All other experiments were repeated multiple times with the similar results.
Data exclusions	No data were excluded from analyses.
Replication	Multiple EM data sets were collected with very similar quality. All other experiments have been repeated multiple times with excellent reproducibility.
Randomization	Experimental groups are not needed for this work, therefore randomization is not relevant.
Blinding	The investigators were blinded to group allocation during data collection and/or analysis because groups were not necessary for this work.

Reporting for specific materials, systems and methods

Materials & experimental systems

n/a	Involved in the study
☒	☐ Unique biological materials
☐	☒ Antibodies
☐	☒ Eukaryotic cell lines
☒	☐ Palaeontology
☒	☐ Animals and other organisms
☒	☐ Human research participants

Methods

n/a	Involved in the study
☒	☐ ChIP-seq
☐	☒ Flow cytometry
☒	☐ MRI-based neuroimaging

Antibodies

Antibodies used	Hybridoma cells for production of an anti-V3 antibody 447-52D was kindly provided by Dr. Susan Zolla-Pazner, New York University. PE Mouse antihuman CD195 (Clone 2D7/CCR5 (RUO), Catalog # 550632, Lot # 5219800; BD Biosciences, San Jose, CA). Anti-His tagged PE conjugated Mouse IgG (Catalog # IC050P, Lot # LHN0316101; R&D Systems, Minneapolis, MN). Anti-CCR5 antibody (Catalog # AB1889, Lot # 2816560; EMD Millipore Corp, USA).
Validation	Antibody 447-52D was tested for binding to HIV-1 gp120. The BD Biosciences website states PE Mouse Anti-Human CD195 is routinely tested by flow cytometry. For anti-His tagged PE conjugated Mouse IgG, the R&D Systems website lists the following citations: T Carmenate et al., J. Immunol., 2018;0(0); DX Bu et al., Oncotarget, 2018;9(40):25764-25780; Bozza S et al., J Immunol, 2014;193(5):2340-8; Sun Y et al., J. Biol. Chem., 2012;287(19):15837-50. The EMD Millipore website states that anti-CCR5 antibody (Catalog # AB1889) was confirmed by western blot analysis of CCR5 in THP-1 whole cell lysate with antiCCR5 (NT) at 1:1000 dilution.

Eukaryotic cell lines

Policy information about cell lines

Cell line source(s)	HEK 293T cells were purchased from ATCC; Expi293F from Thermo Fisher Scientific. 293 T or Expi293F stable cell lines were generated either in Bing Chen's lab at Boston Children's Hospital or at Codex Biosolutions.

Authentication	Each cell line was authenticated for protein expression by western blot and/or flow cytometry, and other functional assays, such as cell-cell fusion and chemokine receptor assays.
Mycoplasma contamination	Mycoplasma contamination is routinely tested for our cell culture and no contaminated cells were ever used for our studies.
Commonly misidentified lines (See ICLAC register)	None.

Flow Cytometry

Plots

Confirm that:

☐ The axis labels state the marker and fluorochrome used (e.g. CD4-FITC).

☒ The axis scales are clearly visible. Include numbers along axes only for bottom left plot of group (a 'group' is an analysis of identical markers).

☐ All plots are contour plots with outliers or pseudocolor plots.

☐ A numerical value for number of cells or percentage (with statistics) is provided.

Methodology

Sample preparation	HEK 293T and Expi293F 293T cells stable cell lines was used. For CCR5 expression analysis 1 million of CCR5 expressing cells were washed with PBS and incubated for 30~40 minutes on ice with PE Mouse antihuman CD195 (BD Biosciences, San Jose, CA) in PBS containing 1% BSA. For CCR5-CD4-gp120 complex detection on the cell surface, 1 million of CCR5 expressing cells were washed with PBS and incubated for 30~40 minutes on ice with CD4 and gp120 at concentrations of 4 µg/ml and 10 4 µg/ml respectively in PBS containing 1% BSA. The cells were then washed twice with PBS containing 1% BSA and stained with Anti-His tagged PE conjugated Mouse IgG (R&D Systems, Minneapolis, MN) at 5 µg/ml. All the fluorescently labeled cells were washed twice with PBS containing 1% BSA and analyzed immediately using a BD FACS Canto II instrument and program FACSDIVA (BD Biosciences, San Jose, CA). All data were analyzed by FlowJo (FlowJo, LLC, Ashland, OR).
Instrument	BD FACSCanto II
Software	Flowjo
Cell population abundance	N/A
Gating strategy	Only gating used during analysis was to separate live and single cell populations.

☐ Tick this box to confirm that a figure exemplifying the gating strategy is provided in the Supplementary Information.